

A COMPARATIVE STUDY BETWEEN NEWTONIAN AND NON-NEWTONIAN
MODELS IN A STENOSIS OF A CAROTID ARTERY

A Thesis

by

TEJASVI KRISHNA KHAMBHAMPATI

Submitted to the Office of Graduate and Professional Studies of
Texas A&M University
in partial fulfillment of the requirements for the degree of

MASTER OF SCIENCE

Chair of Committee,	Kumbhakonam Rajagopal
Co-Chair of Committee,	Devesh Ranjan
Committee Members,	Jay Waton
	Robert Handler
	Anastasia Muliana
Head of Department,	Andreas A. Polycarpou

December 2013

Major Subject: Mechanical Engineering

Copyright 2013 Tejasvi Krishna Khambhampati

ABSTRACT

Blood, the most significant biological fluids plays a very vital role in the human mechanism, in terms of supplying the required nutrients to different parts of the human body, removing waste products and defending the body against infection through the action of antibodies. Therefore, it is imperative that blood flow must be studied in great detail. Hemodynamic analysis of blood flow in vascular beds and prosthetic devices requires the rheological behavior of blood to be characterized through appropriate constitutive equations relating the stress to deformation and rate of deformation. Numerical simulations, although not very accurate, provide an excellent alternative around this difficulty.

As part of the preliminary studies, the Newtonian model of blood was assumed, and wall shear stresses have been plotted at certain critical points. Profiles of wall shear stress were then compared with the experimental results of Ku and Giddens. A numerical investigation of blood flow in stenosed carotid artery of the human body is presented in this thesis. Using a three-dimensional computational model of the stenosis, simulations were performed to capture the Non-Newtonian behavior of blood. The flow is considered as being pulsatile, with appropriate realistic boundary conditions.

A shear thinning model (Carreau's) and a visco-elastic model (Yeleswarapu's Olydroyd-B model) have been employed to predict wall shear stress for the case of a healthy carotid artery and two cases of stenosed carotid artery models (50% and 90% stenosed carotid artery). From these simulation results, it was observed that wall shear stresses predicted by the models at certain critical points are different. Recirculation zones, flow separation and associated negative wall shear stress were observed in certain cases.

DEDICATION

To my parents

ACKNOWLEDGEMENTS

I would like to thank my committee chair, Dr. Rajagopal for being an inspiration, and my co-chair Dr. Devesh Ranjan for his valuable time, encouragement and unconditional patience.

Thanks also to my friends and colleagues and the department faculty and staff for making my time at Texas A&M University a great experience. I want to thank my lab mate, Sarat and my cousin for their support. I also want to thank my friends and my roommates for standing by me through my good times and bad times alike. I need to thank Abhishek and Maruti for their timely help in guiding me in my research. Finally, thanks to my family for their encouragement and their unconditional support.

TABLE OF CONTENTS

	Page
ABSTRACT	ii
DEDICATION	iii
ACKNOWLEDGEMENTS	iv
TABLE OF CONTENTS	v
LIST OF FIGURES.....	vii
LIST OF TABLES	ix
CHAPTER I INTRODUCTION	1
1.1 Carotid artery – structure.....	4
1.2 Carotid stenosis and atherosclerosis.....	5
1.3 Hemodynamics and atherosclerosis	7
1.4 Clinical hemorheology	8
1.5 Evaluation method.....	9
1.6 Objective of the study.....	10
CHAPTER II LITERATURE REVIEW.....	12
2.1 Mathematical models	13
2.2 Influence of shear thinning.....	14
2.3 Effects of viscoelasticity	15
2.4 Flow in arteries.....	16
CHAPTER III COMPUTATIONAL MODELING	19
3.1 Introduction	19
3.2 Software tools.....	19
3.3 Governing equations.....	21
3.4 Non Newtonian constitutive equations.....	22
3.5 Program execution for preliminary validation	25

CHAPTER IV COMPUTATIONAL ANALYSIS	26
4.1 Introduction	26
4.2 Geometric model	26
4.3 Inlet boundary condition	28
4.4 Outlet boundary condition.....	30
4.4 Boundary condition at the wall	30
4.5 Constitutive equations	31
4.6 Preliminary computations.....	31
4.7 Hemodynamics of stenosis	38
4.8 Results and discussion.....	39
CHAPTER V CONCLUSION AND FUTURE WORK.....	49
REFERENCES	53
APPENDIX	58

LIST OF FIGURES

	Page
Figure 1. The carotid artery bifurcation in the neck.....	5
Figure 2. X-ray angiogram of stenosis in a carotid artery.....	6
Figure 3. Meshed healthy carotid artery.....	27
Figure 4. Inlet velocity pulse forms at Common Carotid Artery	29
Figure 5. Simulation of flowrates in a healthy carotid artery.....	32
Figure 6. Plot of Ku and Giddens <i>in vitro</i> measurements of WSS at a point on the wall near the inlet of CCA.	33
Figure 7. Comparison of simulated WSS with experimental data at a point on the wall near the inlet of CCA. (Newtonian).....	34
Figure 8. Comparison of simulated WSS with experimental data at a point on the wall near the inlet of CCA. (Yeleswarapu).	34
Figure 9. Comparison of simulated WSS with experimental data at a point on the wall near the bifurcation at the approach of ICA. (Newtonian)	36
Figure 10. Comparison of simulated WSS with experimental data at a point on the wall near the bifurcation at the approach of ICA. (Yeleswarapu).	36
Figure 11. Contours of velocity magnitude in healthy carotid artery showing the recirculation zone at the bulge of the ICA.....	37
Figure 12. A 50% stenosed carotid artery.	40
Figure 13. A 90% stenosed carotid artery.....	40
Figure 14. Comparison of simulated WSS at a point on the wall near the inlet using all the three models.....	43
Figure 15. Simulation of flowrates in a 50% stenosed carotid artery.	44
Figure 16. Comparison of simulated WSS at a point on the wal at the entry of ICA of 50% stenosed carotid artery using different models.	44
Figure 17. Simulation of flowrates in a 90% stenosed carotid artery	45

Figure 18. Comparison of simulated WSS at a point on the wall at the entry of ICA of 90% stenosed carotid artery using different models	46
Figure 19. Comparison of WSS at the bifurcation of a 90% stenosed carotid artery illustrating flow reversal	47
Figure 20. Filled contours of velocity magnitude for a 90% stenosed carotid artery	48
Figure 21. Contours of velocity magnitude for a 90% stenosed carotid artery	48

LIST OF TABLES

	Page
Table 1. Representative dimensions of the bifurcation model	27
Table 2. List of numerical simulations.....	41

CHAPTER I

INTRODUCTION

A stroke occurs when there is an interruption in the flow of blood to a part of the brain, starving it of oxygen, rapidly leading to brain cell death. A stroke is sometimes called a brain attack or a cerebrovascular accident (CVA). Cardiovascular disease (CVD) is the name for the group of disorders related to the heart and blood vessels which include:

- i. hypertension (high blood pressure)
- ii. coronary heart disease (heart attack)
- iii. cerebrovascular disease (stroke)
- iv. peripheral vascular disease
- v. heart failure
- vi. rheumatic heart disease
- vii. congenital heart disease
- viii. cardiomyopathies.

The most common symptom of a stroke is sudden weakness or numbness of the face, arm or leg, most often on one side of the body. Other symptoms include confusion, difficulty in speaking or understanding speech; difficulty in seeing with one or both eyes; difficulty in walking, dizziness, loss of balance or coordination; severe headache with no known cause; fainting or unconsciousness. Depending on the region of the brain

affected, paralysis, speech impairment, loss of memory and reasoning ability, coma, or even death can result.

Stroke is an emergency, requiring immediate medical attention. An estimated 15 million people suffer from stroke annually, according to a report by the World Health Organization (WHO). According to WHO, an estimated 17.3 million people died from CVDs in 2008, representing 30% of all global deaths. Of these deaths, an estimated 7.3 million were due to coronary heart disease and 6.2 million were due to stroke. By 2030, as many as 23.6 million people may die from CVDs, mainly from heart disease and stroke. These are projected to remain the single leading causes of death. In 2008, diabetes directly contributed to 1.3 million deaths due to CVDs. About 7.5 million or 13% of all deaths can be attributed to raise in blood pressure every year. This includes 51% of deaths due to strokes and 45% of deaths due to coronary heart disease.¹

Stroke carries a high risk of death and is also the leading cause for major disabilities. Risk of recurrence of stroke is high once a stroke has occurred. While one third of new strokes result in death, stroke survivors have long-lasting neurological disabilities requiring rehabilitation or long-term to permanent care. Prompt treatment improves the chances of survival and increases the degree of recovery that may be expected based on the type of stroke suffered.

In recent decades, rapid hospitalization with improved medical facilities and treatment for all types of strokes, have resulted in a dramatic decline in death rate. However, about two-thirds of stroke survivors will have disabilities ranging from moderate to severe. Rehabilitation services may be provided in an acute care hospital,

rehabilitation hospital, long-term care facility, outpatient clinic, or at home. Economically, disabilities have greatly impacted the medical insurance system by pushing up costs for emergency medical care, hospitalization, long term care facilities and institutions. According to the report by the World Health Organization, Disability-adjusted life years (DALYs) can be thought of as “healthy years of life lost”. They indicate the total burden of a disease as opposed to simply the resulting deaths. Stroke burden is projected to raise from around 38 million DALYs globally in 1990 to 61 million DALYs in 2020. The major risk factors for stroke are similar to those for coronary heart disease with unhealthy diet, high blood pressure and tobacco-use, forming the most significant modifiable risks.

Risk of stroke also increases with obesity, high blood cholesterol level, or high red blood cell count. The incidence of stroke is declining in many developed countries, largely as a result of better control of high blood pressure and reduced levels of smoking. However, the absolute number of strokes continues to increase because of the ageing population.

Broadly, strokes are caused either due to ischemia (restricted supply of blood to brain cells due to blood clot or thrombus) or hemorrhages (rupture of blood vessels in the brain). Cerebral thrombosis and cerebral embolism, caused by blood clots that block an artery supplying blood to the brain, either in the brain itself or in the neck, account for 70-80% of all strokes. Subarachnoid hemorrhage and intra-cerebral hemorrhage occur when a blood vessel ruptures leading to bleeding and increased pressure around or in the brain. The risk of death depends on the type of stroke.²

Transient Ischemic Attacks or TIA though resolve in less than 24 hours and have the best outcome, have to be carefully followed up. TIA is followed by stroke caused by carotid stenosis (narrowing of the carotid artery in the neck that supplies blood to the brain). Blockage of an artery is dangerous as the cerebral blood vessel gets ruptured which require immediate medical intervention to prevent fatality. Death of brain cells triggers a chain reaction in which toxic chemicals created by cell death affect other nearby cells. This is one of the reasons why prompt treatment can have a dramatic effect on final recovery. Emergency treatment of stroke due to a blood clot is aimed at dissolving a clot whereas treatment for stroke due to hemorrhages is aimed at controlling the intracranial pressure.²

1.1 Carotid artery – structure

The carotid arteries are two large blood vessels that supply oxygenated blood to the large, front part of the brain. At the throat, the Common Carotid Artery (CCA) branches out into the Internal Carotid Artery (ICA) and the External Carotid Artery (ECA). The internal carotid artery supplies blood to the brain, and the external carotid artery supplies blood to the face shown as Fig.1. At the bifurcation, particularly at the origin of the internal carotid artery, anatomically the vessel expands forming a unique bulb, called the carotid sinus.

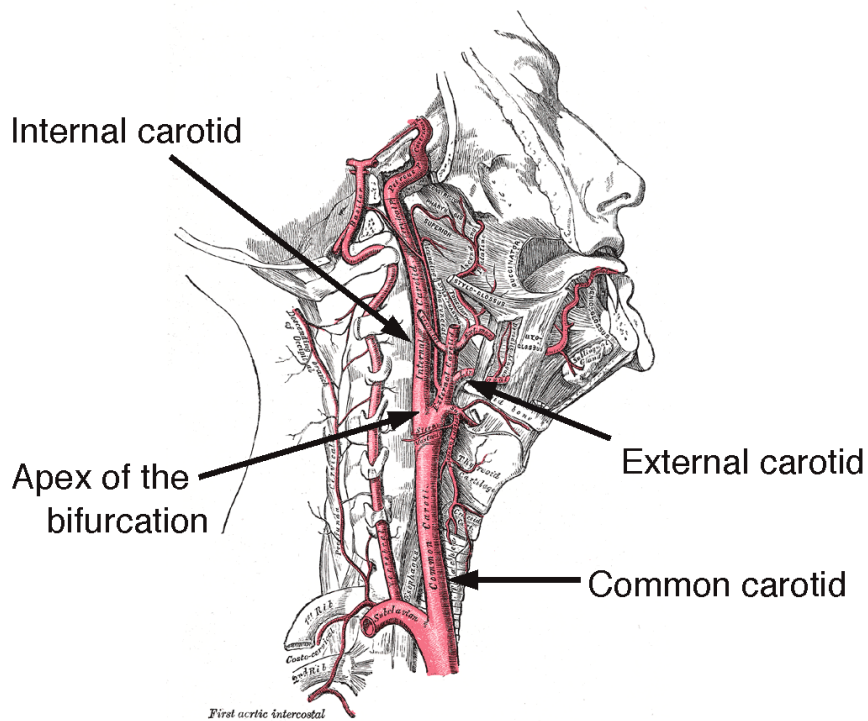


Figure 1. The carotid artery bifurcation in the neck³

1.2 Carotid stenosis and atherosclerosis

Carotid stenosis, which accounts for about 70 – 80% of strokes⁴, is the narrowing of the inner walls of the carotid artery, usually caused by atherosclerosis; an inflammatory build-up of plaque that can narrow the inner walls of the common or internal carotid arteries. Plaque is usually a deposition of cholesterol, and dead fibrous tissues tend to narrow and stiffen arteries due to decreased effective flow diameter and elasticity. The carotid artery bifurcation is a common site for atherosclerosis.

Plaque deposits are usually soft and tend to form irregular areas inside the artery. As this happens, platelets flood the cracked and irregular areas forming blood clots in the carotid artery or one of its branches. Plaque rupture can occur even in lesions that do not

produce significant luminal narrowing or hemodynamic stenosis^{5, 6}. Thus, both through stenosis by the formation of plaque and the formation of blood clots, the carotid artery is a fertile bed for atherosclerosis to thrive. Stenoses are usually defined by the percentage reduction or percentage occlusion of flow radius. An X-ray angiogram of an atherosclerotic carotid artery is shown as Fig.2.

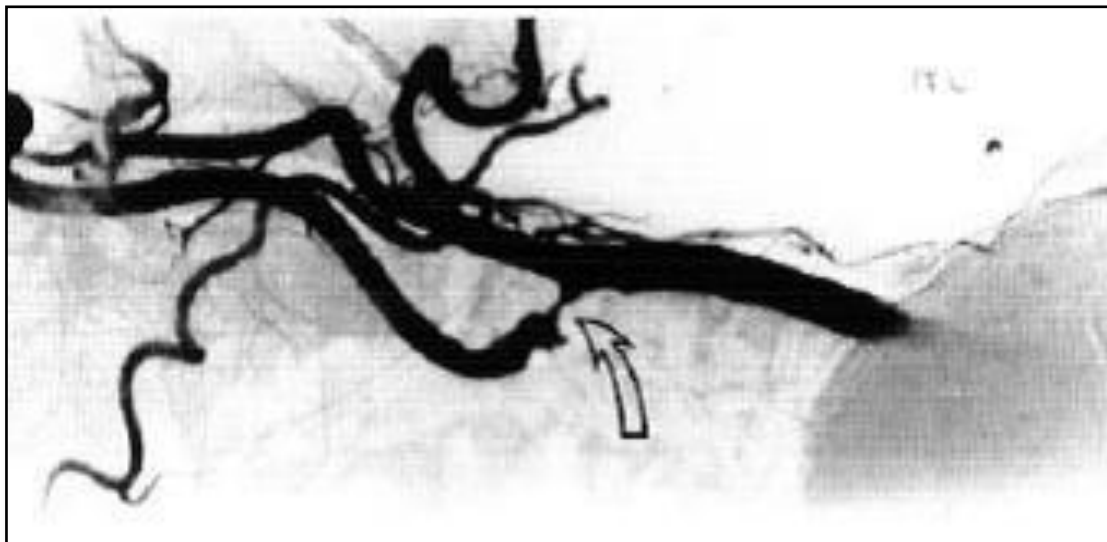


Figure 2. X-ray angiogram of stenosis in a carotid artery

The atherogenic process is enhanced by risk factors: high plasma cholesterol levels particularly low-density lipoprotein, hypertension, smoking, and diabetes. Many clinical laboratory investigations are periodically conducted to help in the management of these risk factors.

Although it has been well established that the pathogenesis of atherosclerosis is closely related to ischemic stroke and ischemic symptoms, it is a complex multifactorial

relationship and still not completely understood. Various studies have shown that vessel morphology and accompanying mechanical hemodynamic factors, such as shear stress patterns, blood rheology, play a key role in the site selectivity of atherosclerotic plaque development.

1.3 Hemodynamics and atherosclerosis

Although it has been long noted that vascular risk factors, such as serum cholesterol and blood pressure, affect the body uniformly, the formation of atherosclerosis in the body is highly site-specific and non-uniform. In fluid-dynamic systems, the geometry of the flow vessel is a key determinant of its flow characteristics. It has been well established that stenoses, bifurcations, and surface roughness are associated with flow disturbances and complex flow^{7, 8}. Fluid flow patterns at branches are highly dependent on geometry, velocities, and flow division ratios. In the case of human physiology, the flow is additionally pulsatile introducing time dependent behaviour. A good analogy to understand the shape of a stenosis and related flow dynamics is to compare it with other flow constrictors such as venturi meter, flow nozzle, or orifice. Hydrodynamic studies of these flow constrictors can directly provide such information as measurements of pressure drop vena-contracta and non-recoverable head loss due to separation and turbulence.

Clinically relevant hemodynamic parameters such as pressure, velocity, blood flow patterns and shear stress, can be directly or indirectly quantified. The relation between wall shear stress and the development of atherosclerosis has been studied using

wall shear stress values derived *in vivo* from phase-contrast Magnetic Resonance imaging (MRI) and pulsed Doppler sonography.

1.4 Clinical hemorheology

Clinical hemorheology deals with pathological abnormalities. It has been developed based on the evidence that the change of rheological properties of blood and its components, might be the fundamental cause for many cardiovascular diseases. Hemorheological alterations are an indicator of insufficient circulatory function.

Blood is a complex fluid of cellular deformable components, viz., red blood cells (erythrocytes), white blood cells (leucocytes) and platelets (thrombocytes), suspended in an aqueous polymer medium called plasma containing proteins, lipids, electrolytes, hormones, enzymes, antibodies and other mineral ions. Particular attention has been paid to the red blood cells due to their significant influence on the mechanical properties of blood.

The study of blood flow in the vascular system is complicated in many respects and thus simplifying assumptions are often made for the purpose of analysis. In large vessels of 1 to 3cm in diameter, where shear rates are high, blood is assumed to have constant viscosity and thus is assumed to be Newtonian. Numerical blood flow studies in these vessels are usually based on the Navier-Stokes equations with an appropriate constant reference viscosity. The Navier-Stokes equation is a momentum equation for Newtonian Fluids. The governing constitutive equation relates the shear stress and shear rate by a constant viscosity which is considered as a Newtonian fluid property.

Plasma is a Newtonian fluid. The rheology of blood is primarily determined by the behavior of erythrocytes at different shear rates due to their presence at a very high concentration comprising about 40 to 45% of blood volume. Deformability, orientation and aggregation of red blood cells (RBC) result in shear thinning viscosity of blood. In smaller vessels (such as arteries and arterioles or veins and veinules with 0.2mm to 1cm diameter) or in some diseased conditions (leukemias, sickle cell anemia, atherosclerosis or hypertension among others) the viscosity of blood is affected, thereby exhibiting remarkable non-Newtonian properties like shear thinning effect and visco-elasticity. Also, studies have shown that Newtonian model could not explain complex flows such as flow through various artificial organs and arterial bifurcations and bends.

Blood is thus, a multi-component mixture with complex rheological characteristics which interacts both mechanically and chemically with vessel walls, giving rise to complex fluid-structure interaction. Thus, pulsatile flow of blood in the cardiovascular system depends, not only on blood rheology but also on the geometry and mechanical properties of the vascular system.

1.5 Evaluation method

Treatment for carotid artery disease normally consists of normalization of those risk factors that cause artery blockages, specific medications (usually antiplatelet medications), and sometimes treatment to open the narrowed carotid artery with an angioplasty and stent, or by a surgical procedure.

Carotid stenosis is usually diagnosed by color flow duplex ultrasound scan of the carotid arteries in the neck. Existence of blockages in the arteries that carry blood to the brain can be determined by Doppler ultrasound. Physicians recommend ultrasound screening for those who have been diagnosed with atherosclerosis or other risk factors for carotid artery disease.

Computed Tomography is used to confirm the diagnosis of stroke and evaluate the cause by hemorrhage in the brain. Magnetic Resonance Angiography (MRA) is a non-invasive diagnostic technique to image the arteries in the brain and further localize the site of the stroke and find the source.

An angiogram is an X-ray in which a contrast agent, or dye, is injected into a vein to highlight the blood vessels to pinpoint the exact location of blockage or bleeding in the brain. Angiography is also used to guide thin tubes called catheters to the site of the problem and administer treatments. In angioplasty, the physician uses a catheter that carries a stent (a balloon-type inflatable tube) to the site of a narrowed or blocked artery. The stent then expands the blood vessel for enhanced blood flow and provide structural support to the artery.

1.6 Objective of the study

The aim of this thesis is to establish a reliable procedure, using FLUENT software, for pulsatile flow simulations to assess wall shear stress in a carotid bifurcation and explore the application of non-Newtonian models for blood in stenosed carotid artery. To investigate the flow dynamics of non-Newtonian models in the case of

stenosed carotid artery bifurcation, two models of stenoses have been created, viz., moderate and acute stenosis with 50% and up to 90% reduction in the flow diameter respectively of the Internal Carotid Artery (ICA). Three models, viz., Newtonian, Carreau shear thinning and Yeleswarapu visco-elastic generalized Oldroyd-B fluid models have been used to study the non-Newtonian behavior of blood in stenosed carotid artery.

CHAPTER II

LITERATURE REVIEW

Numerous investigations⁹⁻¹¹ report that the genesis and the progression of the carotid artery disease, are related with the locally complex and multi-directional flow field in the vicinity of curvatures, branches and bifurcations of large and medium sized blood vessels. Sequeira and Janela⁹ investigated the correlation between hemodynamic factors and atherogenesis. Hemodynamic factors such as flow separation, flow recirculation, or low and oscillatory wall shear stress is now recognized as playing an important role in the localization and development of arterial diseases. According to Cunningham and Gothlieb¹¹, physiological laminar shear stress is crucial for maintaining healthy vascular functions. The fluid drag force acting on the wall is mechano-transduced into a biochemical signal. This biochemical signal regulates the vascular behavior. The combination of flow pulsatility and altered hemodynamics around the arterial curvatures, branches and bifurcations create flow separation and flow recirculation zones inducing low oscillating wall shear stress. These hemodynamic forces promote increased particle residence time at these anatomically unique locations. Such mechanical factors acting along with systemic risk factors (ex: serum cholesterol) promote atherogenesis.

Glagov et al.¹² attributed the selective localization to geometrical and mechanical factors in susceptible blood vessels, noting “the propensity for plaque formation at bifurcations, branching and curvatures has led to conjectures that local

mechanical factors such as wall shear stress and mural tensile stress potentiate atherogenesis.” From the investigations of Jou and Berger¹³, it is known that endothelial cells (surface cells of the blood vessel) can react to changes in shear in a variety of ways, including changes in morphology, proliferation and migration behavior and modulation of the synthesis and secretion of humoral factors (factors transported by blood such as hormones and antibodies) cells. Studies of Prabhakaranetal.¹⁴ have shown that the shape of stenosis plaques and the near wall flow properties play an important role in determining whether a plaque will rupture under the stress produced by changing flow conditions. It has been suggested that irregularly shaped plaques are more likely to rupture and lead to acute coronary syndromes such as ischemia.

2.1 Mathematical models

Mathematical models of blood are difficult to simulate numerically in an efficient manner because blood is made of various components with complex rheological characteristics that regulate its interaction with vessel walls. In blood flow simulations, it is important to describe precisely the nature of blood, as a fluid. Most of the existing literature^{15, 16, 19, 20} modeled blood as a Newtonian fluid. Perktold et al.^{17,18} have shown in their numerical studies that shear thinning properties of blood are not significant for flow in large arteries. Ku and Giddens¹⁹ in their LDA experiments have measured in vitro wall shear stresses in model carotid bifurcation using a Newtonian fluid. A periodic inlet velocity boundary condition was used in their experiments to mimic a pulsatile human cardiac output. The fluid that was used for

LDA experiments is a mixture of water and glycerin having an absolute viscosity of 3.5cP at room temperature. Deshpande et al.²⁰ have shown the flow physics in stenosed carotid arteries with an assumption that blood behaves as Newtonian fluid. Many such studies do not take into consideration the role of the shear-thinning effects and viscoelasticity of blood.

2.2 Influence of shear thinning

First attempts to recognize the shear thinning effects of blood, a non-Newtonian fluid characteristic, were made by Chien et al.^{21, 22}. In vivo determination of wall shear stresses is difficult to accomplish due to the opacity of blood. Hence, accurate modeling is required for improved treatment modalities in vascular disease patients and to provide insight into the cellular biochemical mechanisms that promote the progression of atherosclerosis. Baskurt and Meiselman²³ extensively reviewed the hemodynamics and rheology of blood with a special emphasis on the role of erythrocytes in cellular mechanical properties. RBCs account for a majority of the formed elements in blood. Presence of cellular elements disturbing the flow streamlines is the primary reason for increasing blood viscosity. Normal human blood exhibits shear-thinning behavior. At low shear rates or shear stresses the apparent viscosity is high, whereas the apparent viscosity decreases with increasing shear and approaches a minimum value under high shear forces. At high shear rates above 100 to 200 sec⁻¹, the viscosity of normal blood measured at 37°C is about 4cP to 5cP and is relatively insensitive to further increases of shear. However, the viscosity becomes increasingly sensitive to shear rates below 100

sec^{-1} and increases exponentially as the shear rate is decreased. Thus, blood is assumed to behave as a Newtonian fluid at shear rates above 100s^{-1} and at rates lower than 100s^{-1} , as a non-Newtonian fluid. Shear stresses depend nonlinearly on the deformation rate of erythrocytes.²⁴

Empirical models for shear thinning effects developed by Carreau²⁵, Cross²⁶, Carreau-Yasuda²⁷, and Cason²⁸ with suitable constants were seen to agree well with their predictions of blood viscosity. However, these models are homogenized models and cannot describe the non-homogenous visco-elastic response of RBCs.

2.3 Effects of viscoelasticity

Erythrocytes are essentially elastic membranes filled with a fluid and hence are expected to behave like a viscoelastic fluid, at least under certain flow conditions. Sequeira and Janela⁹ and Baskurt and Meiselman²³ summarized the role of RBCs in explaining the viscoelastic behaviour of blood. Some materials exhibit viscoelastic behavior, which is a combination of fluid-like and solid-like behavior. RBCs have a tendency to aggregate into linear arrays, termed rouleaux, in which they are arranged like stacks of coins. Linear aggregates then interact to form three-dimensional structures. Increased shear disrupts the aggregates, whereas reduced shear favors aggregation. RBC aggregation strongly depends on the type and concentration of macromolecules in the suspending medium. Fibrinogen and other large plasma proteins promote RBC aggregation, with aggregation dependent on the magnitude of shearing forces acting on the cells.

Normal RBCs are highly deformable bodies and tend to orient themselves with the flow streamlines, especially if the shear forces are high enough to deform these cells. RBCs behave as elastic bodies, and thus the shape change is reversible when the deforming forces are removed. However, the RBC membrane can exhibit plastic changes under some pathological circumstances and can be permanently deformed by excessive shear forces.

Many studies have been undertaken to evaluate the viscoelastic nature of blood under conditions of low shear stresses. Thurston^{29, 30} was one of the earliest to recognize the viscoelastic nature of blood. He observed that an increase in shear rate reduces the viscoelasticity of blood. At a given frequency, it was evident that the measured shear rate was non-linear. Thurston^{29, 30} and Quemada³¹ derived a non-linear Maxwell type model of viscoelasticity. Philips and Deutsch³² proposed a three dimensional frame invariant Oldroyd-B model by fitting experimental data from one dimensional blood flows, and generalizing such curve fits to 3 dimensions. Yeleswarapu³¹ has obtained a generalized 5 parameter Oldroyd-B model by conducting similar experiments.

2.4 Flow in arteries

Numerical investigations^{34, 35, 36, 37} of non-Newtonian effects on the pattern and distribution of blood flow in bifurcations, branches and grafts have been reported, but only a few pertaining to carotid arteries. Most of these studies^{35,38,39} reported that under normal physiological conditions non-Newtonian effects do not assume any significance.

Yang and Tang³⁸ studied the comparisons of Newtonian and non-Newtonian assumptions using simple symmetric geometries. Tu and Deville⁴¹ and Lee⁴² simulated the blood flow models through stenoses using Herschel–Bulkley, Bingham and Power-Law fluids in a rigid circular tube with a partial occlusion. Chan et al.⁴³ compared Carreau and Power-Law models with Newtonian model for a 45% stenosis with a trapezoidal profile and concluded that while Carreau and Newtonian models were well within the agreement, the Power-Law model differed significantly from Newtonian model and estimated higher vortices and smaller WSS. Shaw et al.⁴⁴ investigated the Casson fluid flow model for flow of blood through a stenosed bifurcated artery and observed that in both the femoral and coronary arteries, the variation of axial velocity and the flow rate with yield stress is uniform.

Numerical simulations of a stenosed carotid artery were performed by A.Razaviet al.⁴⁵ using various non-Newtonian rheological models and concluded that, at lower velocities the wall shear stresses predicted by non-Newtonian models are higher than those predicted by Newtonian model.

In most of the earlier work, authors have estimated the wall shear stresses considering blood as Newtonian either through simulated experiments or with computational methods. Although extensive literature, on stenosed carotid artery reported using Newtonian and non-Newtonian models, is not available, much work reporting the study of non-Newtonian models employed shear thinning models only. However, blood is known to exhibit both viscoelastic and shear thinning properties for flow in small diameters and at low shear rates. To the best of author's knowledge there

is a dearth of work taking into consideration the viscoelastic nature of blood in stenosed arteries. The present work aims to simulate blood flow in stenosed carotid arteries of varying acuteness taking into consideration, both the viscoelasticity and shear thinning properties of blood.

CHAPTER III

COMPUTATIONAL MODELING

3.1 Introduction

Computational Fluid Dynamics is widely applied for exploratory research of fluid flow in complex geometries with flexibility to incorporate user defined properties. It has immense potential in biomedical applications. Data from patients with different diseases using non-invasive techniques such as intravascular ultrasound can be used to validate relevant hemodynamic flow quantities and generate metrics of the disease state. Patient specific treatment strategies can be developed by providing design-algorithms using such data thus developing new techniques of clinical practice for computer-aided surgical planning in a grid-supported virtual environment.

So it is crucial to develop accurate simulation tools to understand the hemodynamics, especially at the location of diseased arteries. A reliable simulation technique enables the creation of an experimental environment. This facilitates training for virtual invasive techniques like angioplasty and stenting.

3.2 Software tools

DigXY is a digitizer with a simple interface that allows you to extract data of a graph or chart. You can open the graph image in several popular formats, or use built-in scanner support to scan the plot directly into DigXY for digitization. It's easy to digitize values, even if the image is rotated. Also, the software supports linear or logarithmic

axes and works well with contour plots, scatter plots, and photos. Collected data points are shown in a spreadsheet view and can be pasted directly into Microsoft Excel or other text editors.

MATLAB[®] is a high-level language and interactive environment for numerical computation, visualization, and programming. Using MATLAB, one can analyze data, develop algorithms, and create models and applications. The language, tools, and built-in math functions enable one to explore multiple approaches and reach a solution faster than with spreadsheets or traditional programming languages, such as C/C++ or Java[™].

The ANSYS Workbench platform upon which a geometric model is created, meshed and appropriate boundaries are identified and marked. With bi-directional CAD connectivity, powerful highly-automated meshing, a project-level update mechanism, pervasive parameter management and integrated optimization tools, the ANSYS Workbench platform delivers unprecedented productivity, enabling Simulation Driven Product Development.

Ansys Fluent[®] is commercially available CFD software widely accepted for its high reliability. The software has different capabilities and functions. Both 2D and 3D models can be tested with laminar, inviscid, or turbulent flows. Steady and unsteady problems can also be handled using this software. Depending on the model and flow type the designer chooses the appropriate flow field type. Fluent also provides mesh flexibility including the ability to solve complex flow problems using unstructured meshes that can be generated about complex geometries with relative ease. Supported mesh types include 2D triangular or quadrilateral, 3D tetrahedral, hexahedral or

polyhedral meshes and hybrid meshes. Fluent is flexible to allow us to refine or coarsen a grid based as required.

Ansys Fluent® is written in the computer language C and makes use of the flexibility and variety offered by the language. User defined functions (UDF) written in C may also be appended to Fluent, thus increasing its versatility. Fluent uses finite volume discretization method in order to convert Partial Differential Equations of conservation of mass and momentum into non-linear algebraic equations.

3.3 Governing equations

Mass conservation

$$\frac{\partial \rho}{\partial t} + \text{div}(\rho \underline{v}) = 0 \quad (1)$$

Momentum conservation

$$\frac{\partial}{\partial t}(\rho \underline{v}) + \text{div}(\rho \underline{v} \underline{v}) = -\nabla p + \text{div}(\underline{\tau}) + \rho \underline{g} \quad (2)$$

$$\underline{\tau} = \mu \left[\left(\text{grad}(\underline{v}) + \text{grad}(\underline{v})^T \right) - \frac{2}{3} \text{div}(\underline{v}) \underline{I} \right] \quad (3)$$

Where ρ is the density, \underline{v} is the velocity, p is the pressure, $\underline{\tau}$ is the stress tensor and \underline{g} is the body force.

3.4 Non Newtonian constitutive equations

Shear thinning

It is defined as a fluid whose viscosity decreases with an increase in shear rate. Most shear thinning fluids are characterized by distinct linearity at very low and very high viscosity rates. In the shear stress against shear rate plot, the slopes at very low and very high viscosity rates are called as “zero shear viscosity” and “infinite shear viscosity” respectively. Shear thinning fluids is a sub classification of time-independent fluids. Shear thinning models such as Cross and Carreau, are used for modelling time-independent fluids.

Cross Shear thinning model

In order to obtain the required Newtonian region at low and high rates, Cross proposed the Power-Law model,

$$\frac{\eta - \eta_{\infty}}{\eta_0 - \eta_{\infty}} = [1 + (\lambda \dot{\gamma})^m]^{-1} \quad (4)$$

where η is the instantaneous viscosity, η_0, η_{∞} are the zero and infinite viscosities, λ is the time constant and $\dot{\gamma}$ is the shear rate. The values for the constants are $\lambda = 1.007s$, $m = 1.089$, $\eta_0 = 0.56P$ and $\eta_{\infty} = 0.0345P$

Carreau shear thinning model

Another well-known shear thinning model is proposed by Carreau²⁵ is provided here:

$$\frac{\eta - \eta_{\infty}}{\eta_0 - \eta_{\infty}} = [1 + (\lambda \dot{\gamma})^2]^{\frac{n-1}{2}} \quad (5)$$

is the instantaneous viscosity, η_0 and η_∞ are the zero and infinite viscosities, λ is the time constant, $\dot{\gamma}$ is the shear rate and n is the rate law index. The values for the constants are $\eta_0 = 2.415s$, $n = 0.3568$, $\eta_0 = 0.56P$ and $\eta_\infty = 0.0345P$.

Visco-elasticity

It is the property of materials that exhibit both viscous and elastic characteristics when undergoing deformation and exhibit time dependent strain.

Oldroyd-B visco-elastic model

$$\underline{T} = -p\underline{1} + \underline{S} \quad (6a)$$

$$\underline{S} + \lambda \overset{\nabla}{\underline{S}} = n_1 \underline{A} + n_2 \overset{\nabla}{\underline{S}} \quad (6b)$$

$$\overset{\nabla}{\underline{S}} = \frac{d\underline{S}}{dt} - \underline{L}\underline{S} - \underline{S}\underline{L}^T \quad (6c)$$

$$\overset{\nabla}{\underline{A}} = \frac{d\underline{A}}{dt} - \underline{L}\underline{A} - \underline{A}\underline{L}^T \quad (6d)$$

\underline{T} is the traction tensor, p is the hydrodynamic pressure, λ , n_2 , n_1 are parameters, $\overset{\nabla}{\underline{S}}$, and $\overset{\nabla}{\underline{A}}$ are upper convective derivatives defined as shown above, and \underline{L} is the velocity gradient tensor. The 4-parameter Oldroyd-B model could not adequately represent the shear thinning phenomena as well as visco-elastic behavior of blood.

Generalized Oldroyd-B (Yeleswarapu) model

The classical Oldroyd-B fluid does not capture the effects of shear thinning and thickening, hence, a 5-parameter generalized Oldroyd-B model has been developed by Yeleswarapu³³. Hence forth it is referred as Yeleswarapu model.

Yeleswarapu through his experiments indicated that the apparent viscosity of blood at low shear rates (η_0) is very high, and rapidly decreases with increasing shear rate attaining an asymptotic value (η_∞) at about 300sec^{-1} . Since the apparent viscosity function has distance asymptotic values, a generalized viscosity function is of the form $\mu(\kappa) = \eta_\infty + (\eta_0 - \eta_\infty)f(\kappa)$. The relation for $f(\kappa)$ suggested by Yeleswarapu is given as eqn. 6:

$$\mu(\kappa) = \eta_\infty + (\eta_0 - \eta_\infty) \left[\frac{1 + \ln(1 + \Lambda\kappa)}{(1 + \Lambda\kappa)} \right] \quad (7)$$

$$\text{Where } \kappa = \left[\frac{1}{2} \text{tr}(A_1^2) \right]^{\frac{1}{2}}$$

η_0 and η_∞ are asymptotic apparent viscosity as $\kappa \rightarrow 0, \kappa \rightarrow \infty$ respectively. This generalized viscosity function, $\mu(A_1)$ describes the shear thinning appropriately through the material constant Λ . For the simulation the following values for constants have been used: (as determined by Yeleswarapu) $\eta_0 = 0.596\text{s}^{-1}$, $\eta_\infty = 650\text{s}^{-1}$ and $\Lambda = 14.81$.

This equation is applicable for shear-thinning or shear-thickening fluid, depending on the form of generalized viscosity function. $\underline{L} = \text{grad}(\underline{y})$ is the velocity gradient tensor, $A_1 = \underline{L} + \underline{L}^T$ is the first Rivlin-Ericksen Tensor.

3.5 Program execution for preliminary validation

The governing equations (1), (2), (3) are solved iteratively along with the constitutive (4), (5), (6) and (7) equation subjected to the boundary conditions.

Now, as the equations are non-linear and coupled, an iterative process is used starting from an initial guess value for all the variables. Then the solution is allowed to relax to the final solution as the iterations proceed.

So in order to achieve this in FLUENT, a set of solution controls need to be set up. FLUENT 'standard' scheme is used for the pressure interpolation while the convective and viscous terms in the momentum equations are discretized using "Power Law" scheme. SIMPLE algorithm has been used to solve the pressure velocity coupled equations.

CHAPTER IV

COMPUTATIONAL ANALYSIS

4.1 Introduction

The initial task of the present work is to generate a valid numerical baseline simulation for a healthy carotid artery to validate the data for the reliability of the software tools. Towards this objective, all the relevant simulation parameters, such as flow rates and wall shear stresses at critical points for a model of a healthy carotid artery, is compared with *in vitro* experimental LDA data of Ku and Giddens¹⁹ available in the literature. The task is then to estimate the wall shear stress in stenoses of varying acuteness of carotid artery, using non-Newtonian models.

4.2 Geometric model

The geometric model of a healthy carotid artery is created using Ansys®Workbench with the dimensions specified by Perktold et al¹⁸. The computational simulations are carried out with Ansys Fluent®. Representative dimensions of the bifurcation model are provided in Table 1. An image of a healthy carotid artery mesh that is used in the simulation is shown in Fig.3.

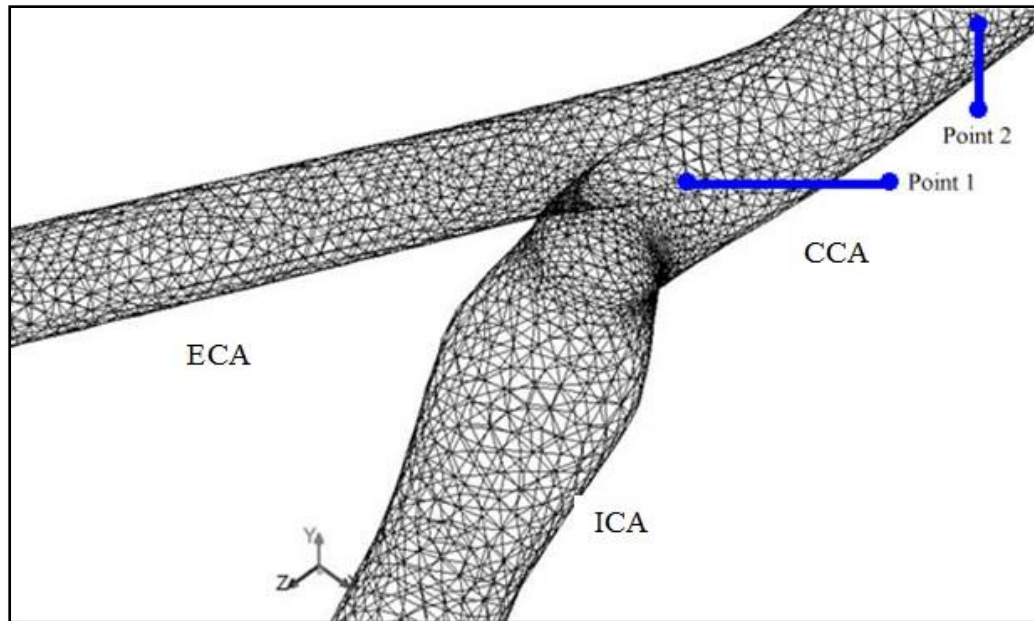


Figure 3. Meshed healthy carotid artery.

Table 1. Representative dimensions of the bifurcation model

S. No.	Parameter	Dimension
1	CCA internal diameter	1.00cm
2	ICA internal diameter	0.75cm
3	Bulge ICA diameter	2.30cm
4	ECA internal diameter	0.65cm
5	ICA bifurcation angle	25.0°
6	ECA bifurcation angle	25.0°

The cross section of the artery is assumed to be circular except at the bulge of ICA and the bifurcation region. The ICA and ECA are extended to thrice the original length to minimize the effect of constant pressure outlet boundary condition that is used in the analysis. An unstructured grid with 87665 cells and 31772 nodes is created to mesh the geometry for simulations. The meshing is finer near the wall to capture the flow in the boundary layer.

Two points are chosen in the domain: point 1 at the wall of proximity of ICA, while point 2 is at the wall of CCA, as shown in Fig. 3. These points are selected to compare values of simulated Wall Shear Stresses (WSS) with *in vitro* LDA measurements available at these points.

4.3 Inlet boundary condition

As the blood flow is pulsatile, the condition for velocity at the inlet is specified as a function of time. Further, the velocity is assumed uniform across the cross section at any instant of time. The velocity waveforms at the entry of CCA are experimentally determined by Holdsworth⁴⁶ and Bloch⁴⁷ are shown as Fig.4. The experimental results of Ku and Giddens¹⁹ consider Holdsworth waveform at the inlet. To validate the computational simulations, the Holdsworth waveform at the inlet is considered in the present analysis.

The velocity profile of Holdsworth waveform is extracted from literature using DigXY® software. The data extracted is utilized for the construction of velocity profile useful in simulation. Towards this, a Fourier series periodic function is constructed,

using Fast Fourier Transform (FFT) in Matlab®. This periodic function is given as input to the model as a User Defined Function (UDF) in C language. The codes developed are listed as appendix.

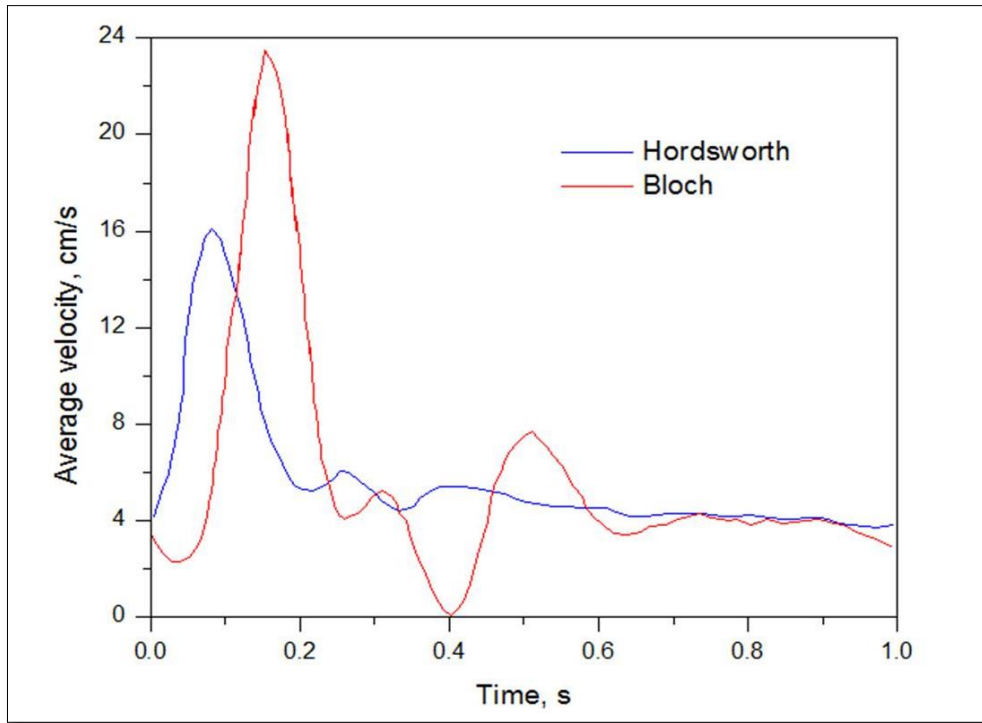


Figure 4. Inlet velocity pulse forms at Common Carotid Artery

$$f(t) = a_0 + \sum_{n=1}^{\infty} \left(a_n \cos \frac{n\pi x}{T} + b_n \sin \frac{n\pi x}{T} \right) \quad (8)$$

Where the coefficients are given as, Note

$$a_0 = 10.387075; a_1 = 1.850111; a_2 = 1.342319; a_3 = 0.898353; a_4 = 0.571498;$$

$$a_5=0.486233; a_6=0.232850; a_7=0.052111; a_8=-0.035078; a_9=-0.091453;$$

$$a_{10}=-0.076763; a_{11}=-0.054678; a_{12}=-0.011458; a_{13}=-0.002826; a_{14}=0.005890;$$

$$a_{15}=0.069500;$$

$$b_1=0.836867; b_2=0.097972; b_3=-0.134835; b_4=-0.301058; b_5=-0.243957;$$

$$b_6=-0.178316; b_7=-0.199582; b_8=-0.188538; b_9=-0.133882; b_{10}=-0.053157;$$

$$b_{11}=0.051542; b_{12}=0.061436; b_{13}=0.096633; b_{14}=0.009737; b_{15}=-0.024491;$$

4.4 Outlet boundary condition

The pressure at the outlet of ICA and ECA is a periodic function of time as the flow of blood is pulsatile. The velocity of blood at the inlet is pulsatile. Consequently the pressure at the outlet is time varying. However, applying time varying velocity inlet condition along with time varying pressure outlet condition makes the problem over determined leading to non-convergence of solution. To resolve this issue the ICA and ECA is extended to thrice the original length and the boundary condition is subjected to atmospheric pressure. This extension of length helps in capturing the pulsatile nature of flow in the carotid artery.

$$P_{outlet} = P_{atm} \quad (9)$$

4.4 Boundary condition at the wall

Blood flow is sensitive to pressure. High pressure in an artery can burst a vessel while low pressure limits the constant supply of nutrients. Elasticity in the arteries helps to dampen the pulses and regulate the pressure. It has been reported that the elasticity of

the wall, varies the wall shear stresses by a maximum of 10%⁴⁸. Hence, in essence, the walls of arteries are elastic but for simulation purpose, it is assumed that the walls are rigid.

$$\frac{\partial v}{\partial r} = 0 \text{ at the wall} \quad (10)$$

4.5 Constitutive equations

For Newtonian model, viscosity is kept at a constant value of 3.5cP, whereas, for the non-Newtonian model, Yeleswarapu model given by Eq.(7) is used in the analysis by developing an UDF given in Appendix.

4.6 Preliminary computations

The purpose of this exercise is to establish and validate all the parameters associated in performing the simulation. Flow rates are computed from simulations at the outlet and wall shear stresses at certain critical points as indicated in Fig.3. The wall shear stresses obtained from these simulations are compared with the experimental measurements made by Ku and Giddens.

For the given flow rate at CCA figure 5 indicates the volume the flow rate through ICA and ECA. The flow rate through ICA is observed to be about two-thirds the flow through CCA. This is because in the case of a healthy carotid artery, the ICA has a bigger diameter as compared to ECA. These outlet flow rates also agree with *in vivo* measurements made by Bharadwaj et al¹⁵.

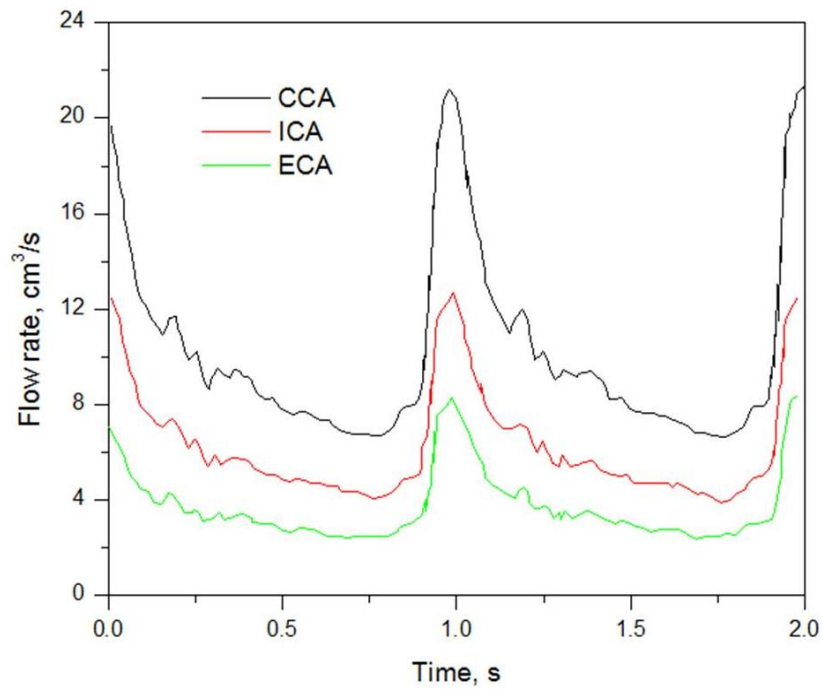


Figure 5. Simulation of flowrates in a healthy carotid artery

Figure 6 indicates WSS measured *in vitro* at a point on the wall of central carotid artery reported by Ku and Giddens. All measurements reported by Ku and Giddens start with the systole, whereas, in the current simulations the inlet boundary condition starts with the diastole.

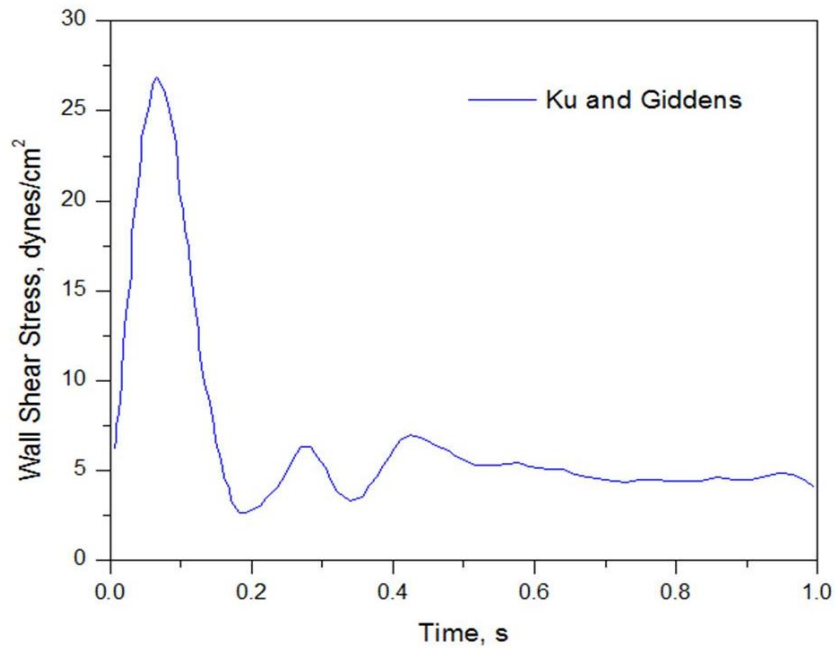


Figure 6. Plot of Ku and Giddens *in vitro* measurements of WSS at a point on the wall near the inlet of CCA.

Hence all results and graphs plotted from these simulations also reflect this phase-difference. However, this phase difference was corrected when comparisons were made during validation. It was noted that WSS remains in phase with inlet velocity in CCA along the wall of CCA until the bifurcation.

Figures 7 and 8 show comparisons of WSS using Newtonian model and Yeleswarapu with LDA experimental results of Ku and Giddens respectively. It can be observed from these plots that there is a good agreement between computed WSS from the simulations and LDA experimental data, although some amount of deviation is witnessed at the systole of the pulse in both cases

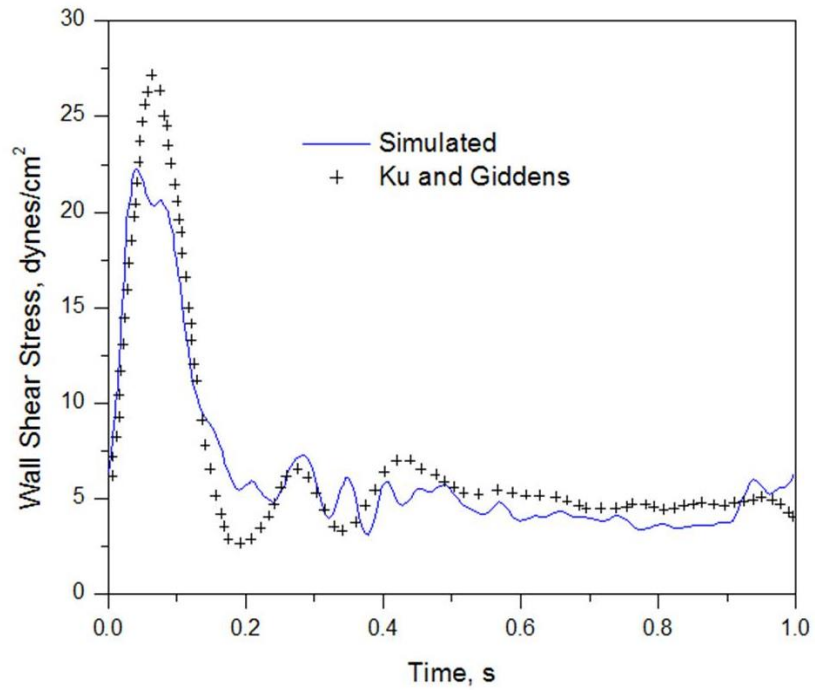


Figure 7. Comparison of simulated WSS with experimental data at a point on the wall near the inlet of CCA. (Newtonian)

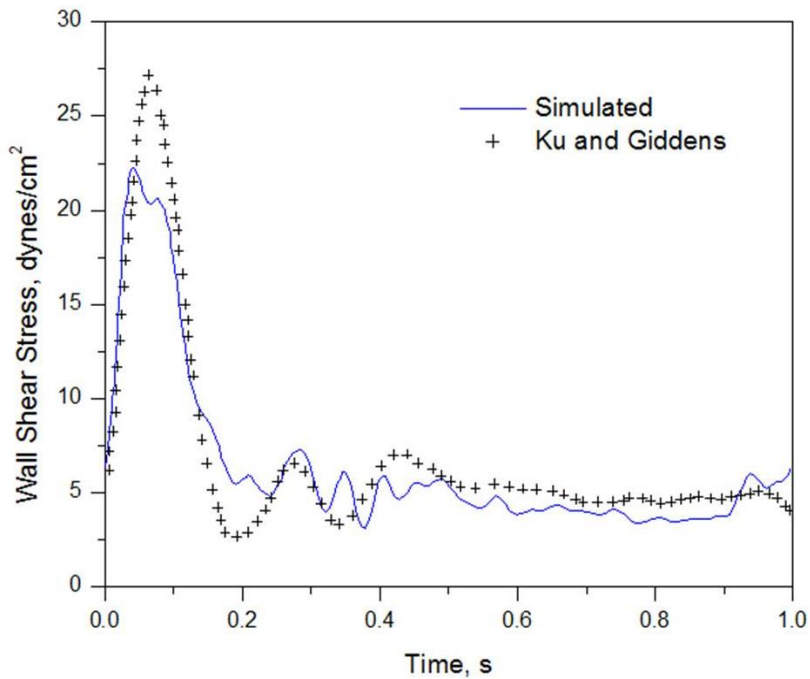


Figure 8. Comparison of simulated WSS with experimental data at a point on the wall near the inlet of CCA. (Yeleswarapu).

The WSS predicted by both Newtonian and Yeleswarapu's models are identical at this point. Bio-adhesion, which is responsible for the non-Newtonian behavior of blood, does not affect the flow in larger diameters. It is expected from the simulations that for flow diameters as big as a healthy carotid artery, the choice of Newtonian or non-Newtonian model does not really bear any significance on the simulations. This exercise reinforces the assumption.

WSS in the proximal ICA at the wall has been plotted in fig. 9 and fig. 10 using Newtonian and Yeleswarapu model respectively. From the plot, it can be observed that there is a sudden reversal in the sign of WSS values during systole. Figures 9 and 10 show comparisons of wall shear stresses using Newtonian and non-Newtonian (Yeleswarapu model) models with LDA experimental results of Ku and Giddens, respectively.

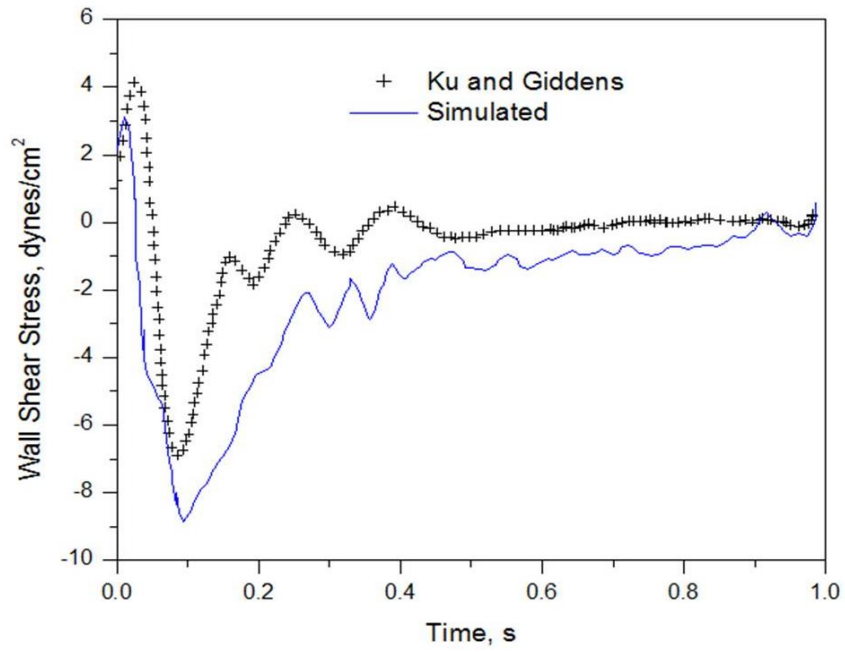


Figure 9. Comparison of simulated WSS with experimental data at a point on the wall near the bifurcation at the approach of ICA. (Newtonian)

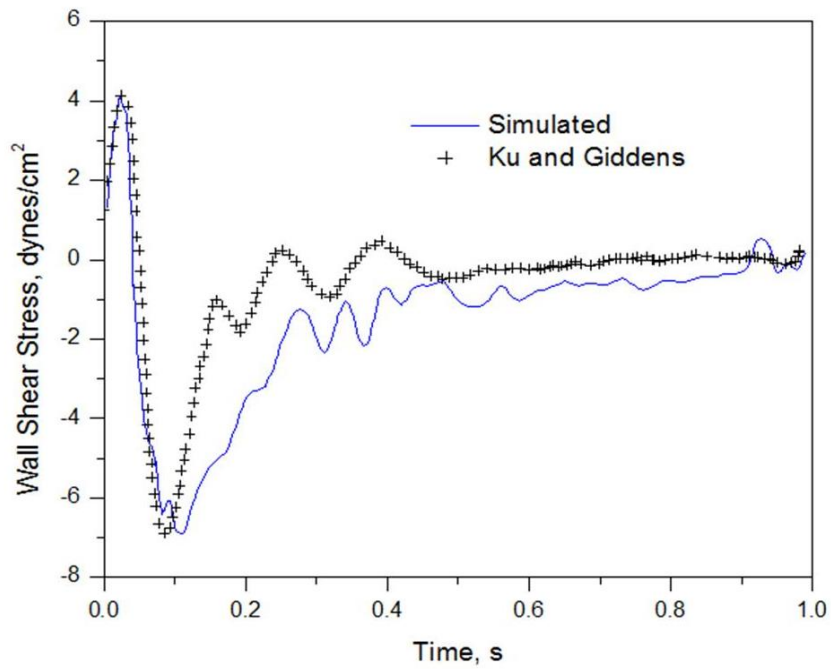


Figure 10. Comparison of simulated WSS with experimental data at a point on the wall near the bifurcation at the approach of ICA. (Yeleswarapu).

From figures 9 and 10, it can also be observed that there exists a small difference in the WSS plots corresponding to flow reversal (at point1 in fig. 3). The magnitude of DEWSS as computed by Yeleswarapu's model at both points of flow reversal is greater than that computed using the Newtonian model. This could be due to the fact that non-Newtonian behavior of blood is more prominent at lower shear rates.

Figure 11 shows the velocity contours by magnitude of the flow-domain at the diastole of the pulse. Regions of recirculation can be seen in the figure.

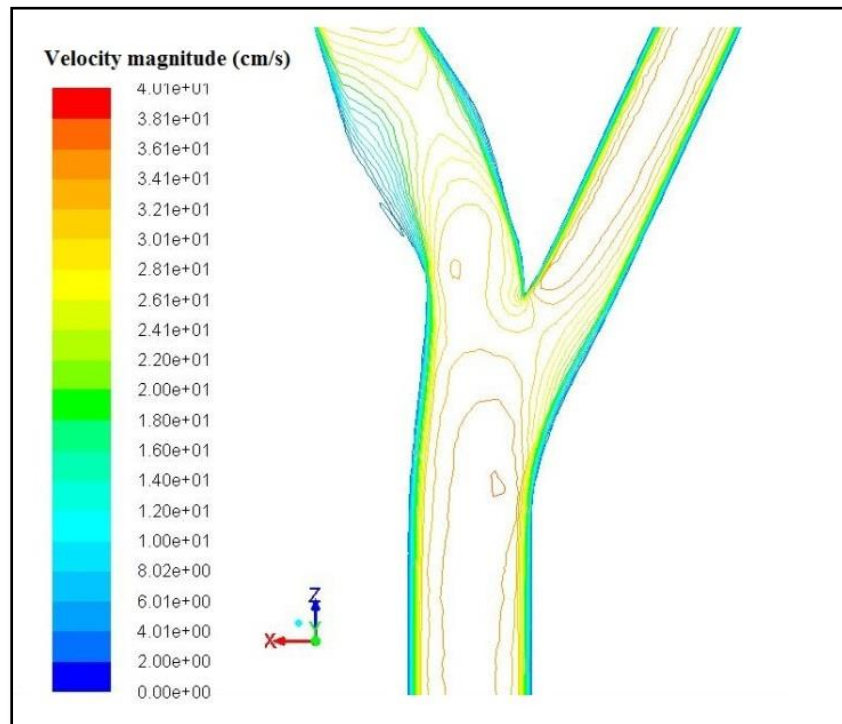


Figure 11. Contours of velocity magnitude in healthy carotid artery showing the recirculation zone at the bulge of the ICA.

4.7 Hemodynamics of stenosis

As the disease progresses, the percent stenosis (defined by reduction in radius) also increases. Velocity in an artery, though, is not a linear function of percent stenosis. For high percentage stenoses, pressure losses generally become significant. Like in a case of an expanding nozzle, flow separation occurs in the expansion region for high percentage stenosis. Because of choking flow that exists in extreme or severe stenoses, flow separation occurs at low Reynolds number 10 or less. It is observed that a strong shear layer develops between the central jet and the recirculation region. The critical upstream Reynolds number for turbulence is approximately 300. Due to pulsatility, turbulence is generated intermittently. For stenoses greater than 75%, several mechanisms severely limit flow. Turbulence downstream of the stenosis is very large and creates significant resistance. The critical Reynolds number greater for turbulence, rapidly falls for stenoses greater 25%. At 50% stenosis, turbulence is generated throughout the pulsatile cycle. At higher levels of stenosis, turbulence is severe and accounts for majority of pressure loss.

Flow separation can also contribute to pressure loss and is a major factor at lower percent stenoses. For a moderate level of stenosis, separation occurs at much lower Reynolds numbers. Separation is a common event in stenoses. A strong shear layer at the interface of the separation region and the central jet creates addition viscous losses. The throat of the stenosis is a site of high shear rates at the wall, which also contribute to viscous losses. For low grade stenoses, the wall and separation shear layers produce

most of the losses. However for high grade stenoses turbulence is the major loss mechanism.

4.8 Results and discussion

Using Ansys Fluent® and C supported UDFs, a series of simulations have been carried out to study the flow behavior of blood through a stenosed carotid artery and to investigate the significance of the non-Newtonian effect on blood flow for various cases of stenotic severity. The boundary conditions for this purpose are the same as those described in the case of a healthy carotid artery. In this section, the results are presented for certain cases to demonstrate the essential features of the blood flow through a stenosed carotid artery and to show the significance of non-Newtonian effect on blood flow for the examined cases. Models used are Newtonian, Carreau and Yeleswarapu. Two models of stenosis are created, one with the diameter reduced by 50% (fig.12) in internal carotid artery, another is an extreme case of stenosis with the diameter reduced by 90% (fig.13).

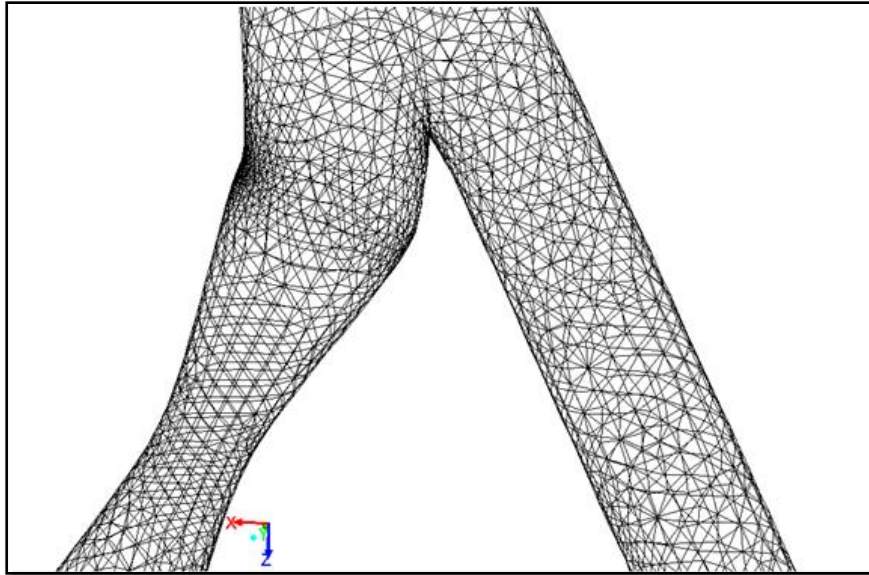


Figure 12. A 50% stenosed carotid artery.

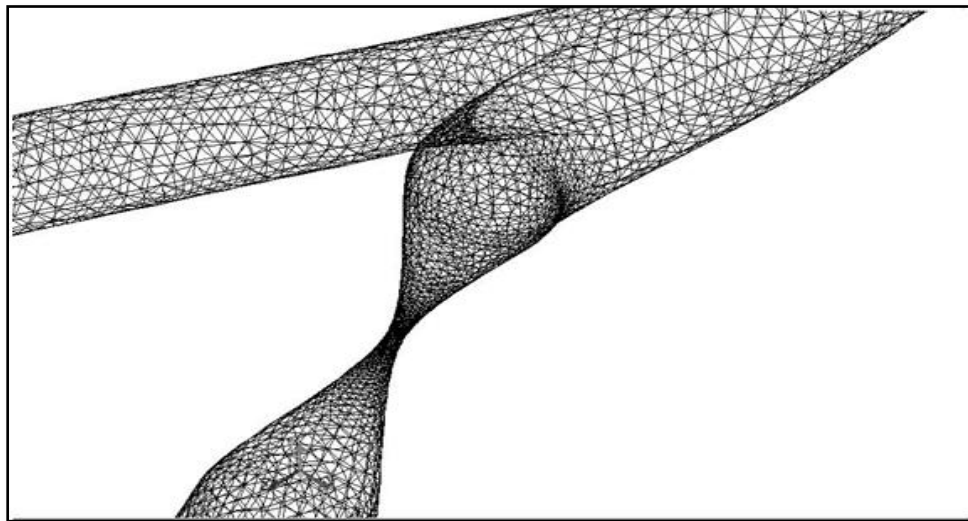


Figure 13. A 90% stenosed carotid artery.

Table 2. List of numerical simulations.

Case #	Description	Constitutive model	Comparison of Wall shear stresses in CCA	Comparison of Wall shear stresses in ICA
1	Healthy Carotid Artery	Newtonian	All models predict WSS with insignificant deviation from each other.	WSS predicted by Visco-elastic slightly greater than Power-Law slightly greater than Newtonian model.
		Carreau		
		Yeleswarapu		
2	50% Stenosed Carotid Artery	Newtonian	All models predict WSS with insignificant deviation from each other.	WSS predicted by Visco-elastic slightly greater than Power-Law greater than Newtonian model (by ~25%).
		Carreau		
		Yeleswarapu		
3	90% Stenosed Carotid Artery	Newtonian	All models predict WSS with insignificant deviation from each other.	WSS predicted by Visco-elastic slightly greater than Power-Law greater than Newtonian model (by ~33%).
		Carreau		
		Yeleswarapu		

For the healthy carotid artery, WSS are plotted at a point on the wall of the CCA that is at the main artery, before it branches out into ICA and ECA. Figure 14 shows the comparison between all the three models at this point. From the figure, it can be observed that all the above mentioned models at this point show similar results. The non-Newtonian behavior is most evident at lower velocities and thinner flow diameters, when the red blood cells clump together into larger particles. Blood usually exhibits non-Newtonian behavior in small branches, where the cells squeeze through and a cell-free skimming layer reduces the effective viscosity through the tube. However, around the region of bifurcation, it is interesting to note that the wall shear stress predicted by Yeleswarapu model is visibly larger than that predicted by Carreau's model, which is slightly greater than that predicted by the Newtonian model.

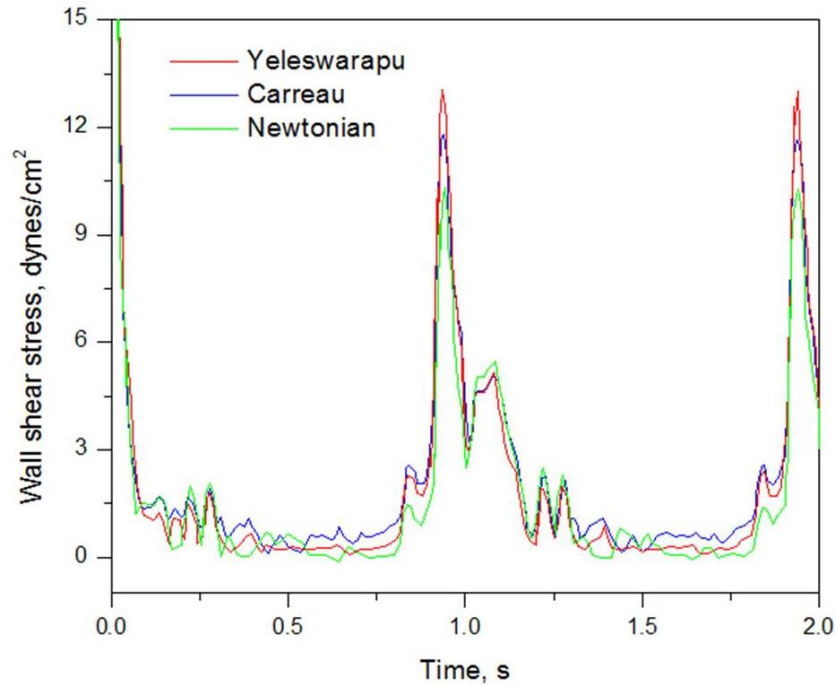


Figure 14. Comparison of simulated WSS at a point on the wall near the inlet using all the three models.

Figure 15 shows the flow distribution for a 50% stenosed artery in ICA. At the wall of CCA, it has been noted that the WSS predicted by all three models is similar. These results are similar to the WSS profiles in a healthy carotid artery. This is also a reasonable observation as the flow diameter is the same as in the case of a healthy carotid artery. In the region around the bifurcation (as shown in fig. 16), the WSS predicted by Yeleswarapu fluid model is visibly larger than that predicted by Carreau model, which is slightly greater than that predicted by Newtonian model. This is consistent with the reasoning from the above paragraph.

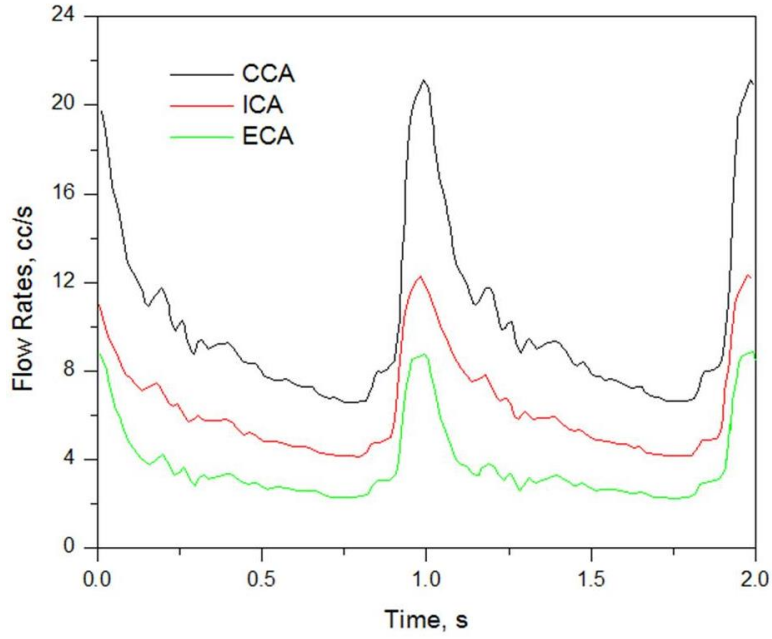


Figure 15. Simulation of flowrates in a 50% stenosed carotid artery.

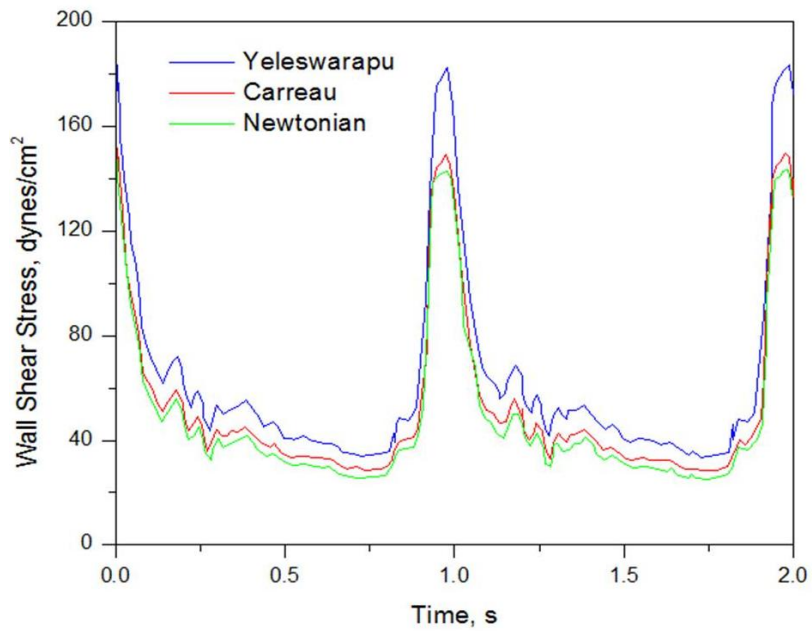


Figure 16. Comparison of simulated WSS at a point on the wal at the entry of ICA of 50% stenosed carotid artery using different models.

An attempt to simulate blood flow in an acute stenosed flow with reduction of diameter by 90% is detailed here. This stenosed artery is choked, causing very little outflow through the ICA (fig. 17 shows flow distribution). WSS is plotted in fig. 18 on the proximal ICA using Newtonian, Carreau and Yeleswarapu models. The WSS is observed to be considerably lower than the WSS in the case of healthy carotid simulation and is also lower than the WSS in the case of 50% stenosed carotid artery. This result is reasonable because in the case of extreme stenosis, the flow rates through the ICA are considerably lower.

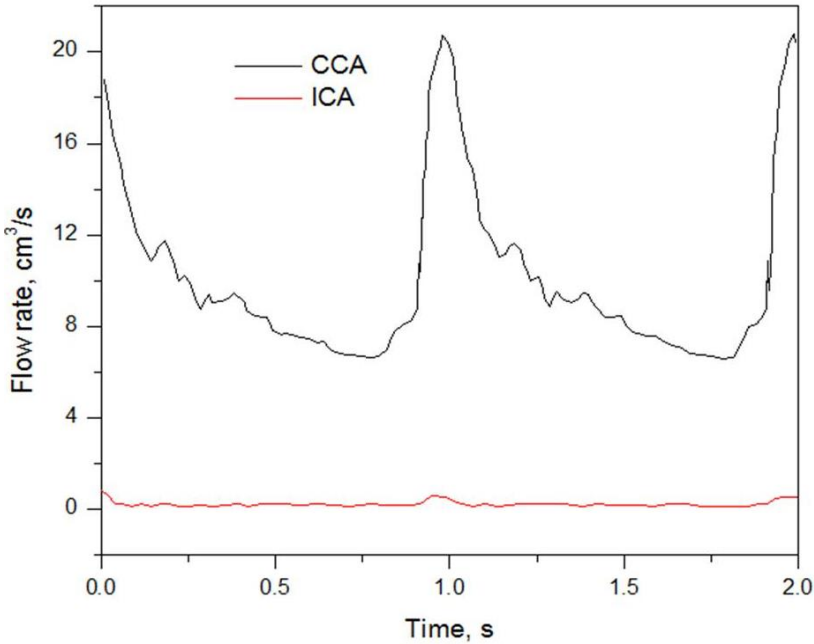


Figure 17. Simulation of flowrates in a 90% stenosed carotid artery

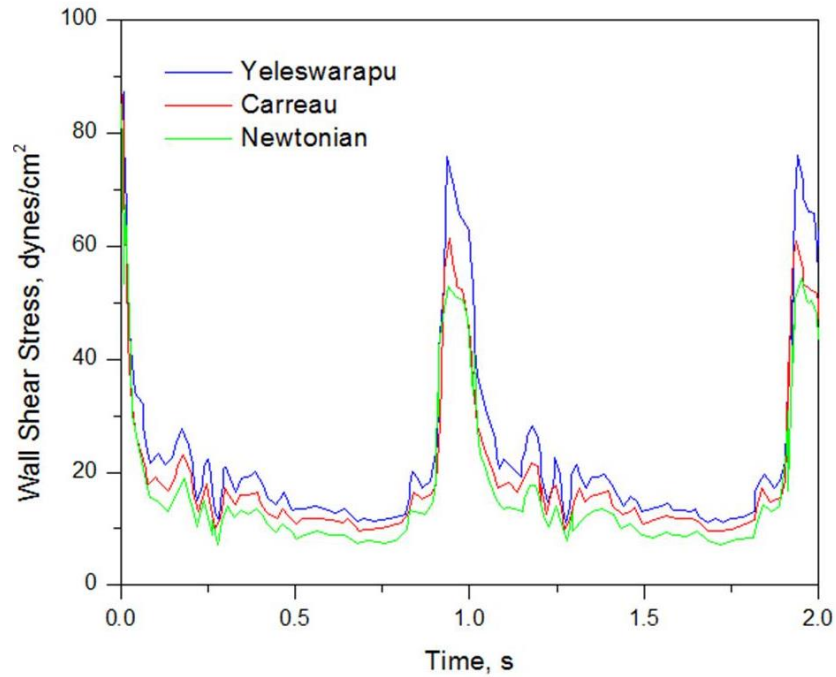


Figure 18. Comparison of simulated WSS at a point on the wall at the entry of ICA of 90% stenosed carotid artery using different models

WSS were plotted at the bifurcation where there is reversal of flow using all three models. It is observed to exist a permanent flow reversal unlike what has been witnessed at the same point of a healthy carotid artery. Another point of note is that the WSS here are relatively very high with peak WSS being close to 500 dynes/cm² in Fig.19. At these high shear rates the WSS predicted by all the three models do not show any clearly distinguishable deviations. At higher shear rates, the clumping of blood cells would be minimal decreasing the non-Newtonian behavior of blood.

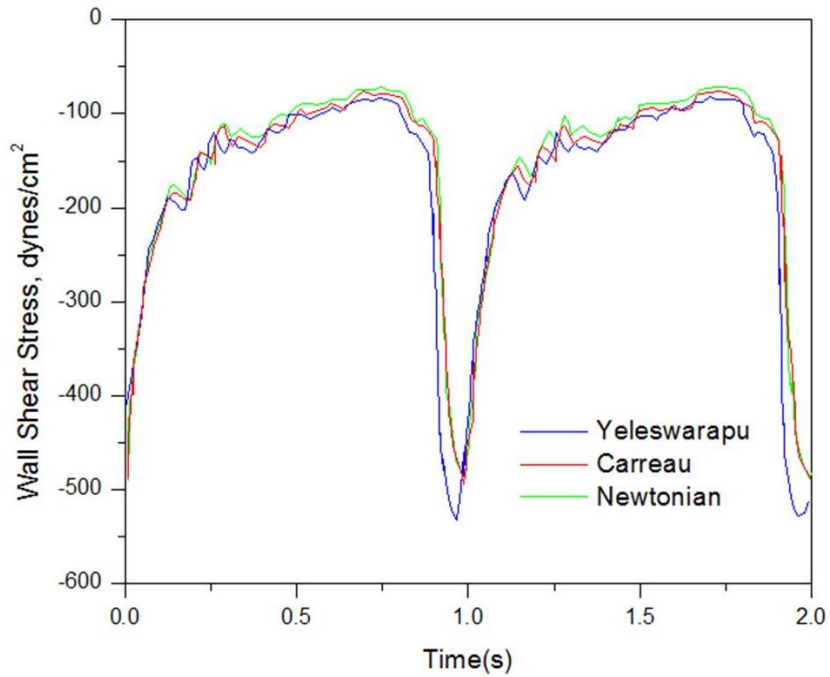


Figure 19. Comparison of WSS at the bifurcation of a 90% stenosed carotid artery illustrating flow reversal

Filled contours of velocity by magnitude are provided below in figures 20 and 21. In Fig. 20, it can be seen that flow reversal occurs at the opening of the ECA. As this is a scenario of extreme stenosis, the ICA allows very little flow. Because a larger fraction of the mass flow is directed into the ECA, there is a case of increase in velocity due to a contracting cross section, i.e. CCA to ECA. This explains the formation of a flow separation zone at the mouth of the ECA. Figure 21 shows the line contours of the domain by velocity magnitude. The flow separation region is zoomed for greater clarity.

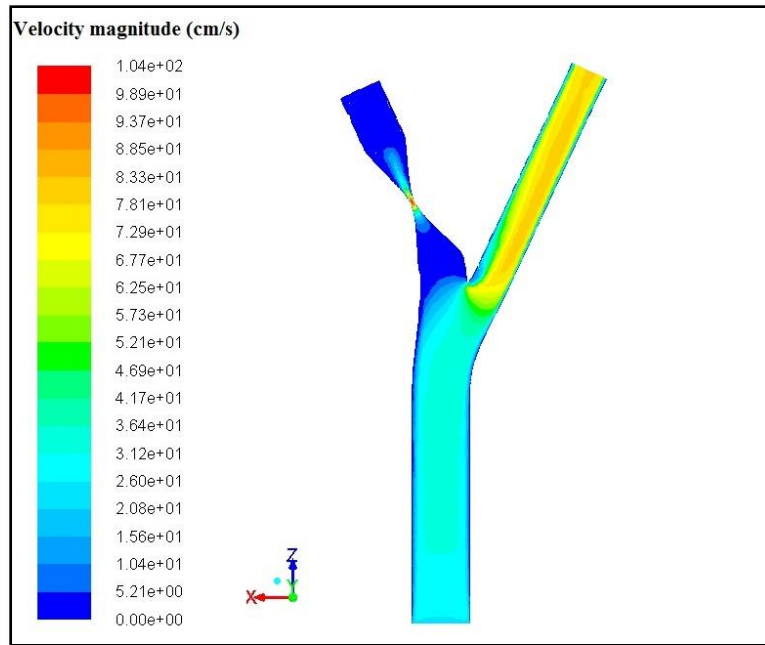


Figure 20. Filled contours of velocity magnitude for a 90% stenosed carotid artery

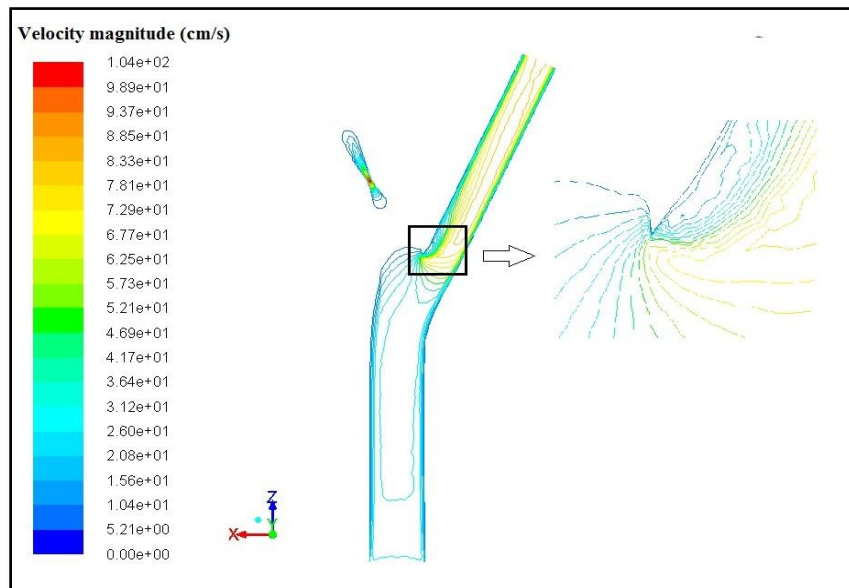


Figure 21. Contours of velocity magnitude for a 90% stenosed carotid artery

CHAPTER V

CONCLUSION AND FUTURE WORK

- 1) To study the flow physics in stenosed carotid arteries, three models of the artery are used. For the purpose of these computations, a healthy carotid artery, 50% stenosed carotid artery and 90% stenosed carotid artery were selected.
- 2) To validate the numerical simulations with experimental data, a healthy carotid artery was simulated using Ansys Fluent®. Wall shear stresses were plotted using Newtonian model and visco-elastic non-Newtonian model (Yeleswarapu model) compared to LDA experiments conducted by Ku and Giddens. The observed WSS profiles showed good agreement with experimental data.
- 3) For simulating the above two stenosed geometries, three viscosity models were used, i.e. the Newtonian model, the shear thinning model (Carreau model), the visco-elastic model (Yeleswarapu model). It was observed that there is no major difference between the WSS predicted in a healthy carotid artery and 50% stenosed carotid artery until the point of stenosis (figures 15 and 17). However, in the case of 90% stenosed carotid artery the flowrate in ICA reduced considerably, decreasing the shear rates and WSS.
- 4) Non-Newtonian models become prominent for the case of 90% stenosis (fig.19). In case of acute stenosis, the flow reversal region shows permanent flow reversal throughout the pulse, whereas, in the case of healthy carotid artery or even a 50% stenosed carotid artery, the flow reversal occurs intermittently in the course of the

pulse. As the WSS computed by Yeleswarapu model or Carreau model are higher than that computed using Newtonian assumption, as the region of stenosis is approached, it can be deduced that the non-Newtonian model predicts a greater stenosis growth rate. This is because the growth of stenosis tends to be greater due to larger WSS that results in a greater tendency for the accumulation of fatty cells.

Some of the possible future endeavors to improve the accuracy of prediction of blood flows include:

- 1) Performing experiments to validate the results of these simulations. One challenge in working with blood flow is that blood cannot be employed as the working fluid because it is opaque. This will cause difficulty in optical access, and any experimental technique that employs optical imaging will be ineffective.
- 2) A solution to this challenge lies in employing a fluid analog to blood that emulates the properties of blood. Two such standout properties of blood are its shear thinning property and Visco-elasticity. As discussed above in section 1, RBCs determine the rheological behavior of blood; both shear thinning and viscosity are related to aggregation, deformation and alignment of the RBCs. An ideal analog needs to mimic both these properties. Finally, since refractive index and viscosity are known to be temperature dependent, it is important to attain both properties at the same working temperature. There are various possibilities of constructing a blood fluid analog.

- a. Experimental techniques such as PIV can be used with a working fluid comprising of glycerol and water (Nguyen et al⁴⁹). However, to attain a refractive index ≥ 1.40 requires at least 40% (by volume) of glycerol, which results in a dynamic viscosity > 5.0 cP at 20°C (i.e. > 80 th percentile of average human blood viscosity), and the higher concentrations needed for larger refractive index will result in even higher viscosity.
 - b. Another possible fluid which has been modeled empirically by Nguyen et al. (uses combinations of diethyl phthalate (DEP) and ethanol could be used with a wide range of refractive index and viscosity values at different temperatures.
 - c. Aqueous Xanthan gum solutions have proven to be one of the more successful blood analog fluids (Brookshier and Tarbel⁵⁰). A concentrated solution of potassium thiocyanate in water (KSCN, 71% by weight) agrees with optical properties and by itself the solution is a Newtonian with kinematic viscosity $\eta = 2.9 \times 10^{-3}$ Pas and density $\rho = 1410 \text{ kg/m}^3$ pretty close to the average blood properties. Addition of 250ppm of Xanthan gum results in shear thinning and visco-elastic behavior of the fluid. Xanthan gum solution (KSCN-X) mimics the shear thinning properties of blood quite well but did not agree with the visco-elastic properties as well. Shear thinning in this case is consistent with the Carreau-Yasuda model.
- 3) In the case of severely stenosed blood vessels, stents have been employed as solution to improve the overall blood flow. A major factor in this phenomenon is the design

of the stent and its effect on blood flow physics, and WSS in particular. Numerical simulations and experiments can be performed to optimize the stent design parameters, using non-Newtonian models. The designs thus improved will have great practical significance and utility in the biomedical field.

REFERENCES

1. Stroke, "Cerebrovascular accident." Accessed 11-10-2012. <<http://www.emro.who.int/health-topics/stroke-cerebrovascular-accident>>.
2. Stroke. "Causes and Symptoms." Accessed 11-10-2012. <<http://medical-dictionary.thefreedictionary.com/stroke>>.
3. Image. Accessed 4-6-2013. <<http://en.wikipedia.org/wiki/File:Gray507.png>>
4. Carotid Artery Disease, Stroke, Transient Ischemic Attacks. "What is Carotid Disease?" Accessed 3-4-2013. <[http://www.vascularweb.org/vascularhealth/Pages/carotid-artery-disease,-stroke,-transient-ischemic-attacks-\(-tias\)-.aspx](http://www.vascularweb.org/vascularhealth/Pages/carotid-artery-disease,-stroke,-transient-ischemic-attacks-(-tias)-.aspx)>.
5. Wasserman, B.A., R.J. Wityk, H.H. Trout, and R. Virmani. 2005. "Lowgrade carotid stenosis: looking beyond the lumen with MRI." *Stroke*. 36: 2504-2513.
6. Hankey, G.J., K. Jamrozik, R.J. Broadhurst, S. Forbes, and C.S. Anderson. 2002. "Long-term disability after first-ever stroke and related prognostic factors in the Perth Community Stroke Study." 1989-1990. *Stroke*. 33: 1034-1040.
7. Granger R.A. 1995. Fluid Mechanics. Dover, New York
8. Bakker P.G. 1991. Bifurcations in Flow Patterns: Some Applications of the Qualitative Theory of Differential Equations in Fluid Dynamics. Springer, New York.
9. Sequeira, A. and J.Janela. 2007. A portrait of research at the Technical University of Lisbon. Springer-Verlag.
10. Cunningham. K.S., A.I. Gotlieb. 2005. "The role of shear stress in the pathogenesis of atherosclerosis." *Laboratory Investigation*. 85: 9-23.
11. Gibson. C.M., L. Diaz, K. Kandarpa, F.M. Sacks, R.C. Pasternak, T. Sandor, C. Feldman and P.H. Stone. 1993. "Relation of vessel wall shear stress to atherosclerosis progression in human coronary." *Arterioscler Thromb Vasc Biol*. 13: 310-315

12. Glagov, S., C. Zarins, D.N. Giddens and D.N. Ku. 1988. "Hemodynamics and atherosclerosis: Insights and perspectives gained from studies of human arteries." *Arch Pathol Lab Med.* 112: 1018-1031.
13. Berger. S.A., L.D. Jou. 2000. "Flows in stenotic vessels." *Annual Reviews of Fluid Mechanics.* 32: 347–382.
14. Prabhakaran S., T. Rundek, R. Ramas, M.S. Elkind, M.C. Paik, B. Boden-Albala, R.L. Sacco. 2006. "Carotid plaque surface irregularity predicts ischemic stroke: the Northern Manhattan Study." *Stroke.* 37: 2696-2701.
15. Bharadvaj, B.K., R.F. Mabon, D.P. Giddens , 1982. "Steady flow in a model of the human carotid bifurcation. Part II: Laser-Doppler measurements." *Journal of Biomechanics.* 15: 363–378.
16. Palmen, D.E.M., F.J.H.Gijsen, F.N. van de Vosse, J.D. Janssen.1997. "Diagnosing minor stenoses in carotid artery bifurcation models using the disturbed velocity field." *Journal of Vascular Investigation.* 3 (1): 26–41.
17. Perktold, K., D. Hilbert. 1986. "Numerical simulation of pulsatile flow in a carotid bifurcation model." *Journal of Biomedical Engineering.* 8: 193–199.
18. Perktold, K., R.O. Peter, M. Resch, G. Langs. 1991. "Pulsatile non-Newtonian flow in three-dimensional carotid bifurcation models: a numerical study of flow phenomena under different bifurcation angles." *Journal of Biomedical Engineering.* 13: 507–515
19. Ku, D.N. and D.P. Giddens. 1987. "Laser Doppler anemometer measurements of pulsatile flow in a model carotid bifurcation." *Journal of Biomechanics.* 20: 407–421.
20. Deshpande, M.D., V. Ballal, S.R. Shankapal, V.M.D. Prabhu, M.G. Srinath. 2009. "Subject specific blood flow simulation in the human carotid artery bifurcation." *Current science.* 97: 1303-1311.
21. Chien, S., S. Usami, R.J. Dellenback, M.I. Gregersen. 1967. "Blood viscosity: Influence of erythrocyte deformation." *Science.* 157 (3790): 827-829.
22. Chien, S., S. Usami, R.J. Dellenback, M.I. Gregersen. 1967. "Blood viscosity: Influence of erythrocyte deformation." *Science.* 157 (3790): 829-831.
23. Baskurt. O.K. and H. J. Meiselman. 2003. "Blood rheology and hemodynamics." *Seminars in Thrombosis and Haemostasis.* 29 (5): 435–450

24. Ku, D.N. 1997. "Blood flow in arteries." *Annual Review of Fluid Mechanics*. 29: 399-434.
25. Carreau, P.J. 1960. PhD Thesis, University of Wisconsin, Madison.
26. Cross, M. M. 1965. "Rheology of non-Newtonian fluids: a new flow equation for pseudoplastic systems." *J. Colloid Sci.* 20: 417-437.
27. Vlastos, G., D. Lerche, B. Koch. 1997. "The superimposition of steady and oscillatory shear and its effect on the viscoelasticity of human blood and a blood-like model fluid." *Biorheology*. 34(1): 19-36.
28. Scott-Blair, G. W. 1959. "An equation for the flow of blood, plasma and serum through glass capillaries." *Nature*, 183: 613-614.
29. Thurston, G. B. 1972. "Viscoelasticity of human blood." *Biophys. J.*, 12: 1205-1217.
30. Thurston, G. B. 1972. "Rheological parameters for the viscosity, viscoelasticity and thixotropy of blood." *Biorheology*. 16: 149-162.
31. Quemada, D. A. 1993. "A non-linear Maxwell model of biofluids - Application to normal blood." *Biorheology*. 30(3-4): 253-265.
32. Phillips, W. M., W.M. Deutsch. 1975. "Towards a constitutive equation for blood." *Biorheology*. 12(6): 383-389.
33. Yeleswarapu, K.K. 1996. "Evaluation of continuum models for characterizing the constitutive behavior of blood". Ph.D. thesis, Department of Mechanical Engineering, University of Pittsburgh.
34. Chen, J., X.Y. Lu, W. Wang. 2006. "Non-Newtonian effects of blood flow on hemodynamics in distal vascular graft anastomoses." *Journal of Biomechanics*. 39:1983–1995.
35. Soulis, J.V., G.D. Giannoglou, Y.S. Chatzizisis, T.M. Farmakis, G.A. Giannakoulas, G.E. Parcharidis, G.E. Louridas. 2006. "Spatial and phasic oscillation of non-Newtonian wall shear stress in human left coronary artery bifurcation: an insight to atherogenesis." *Coron Artery Dis*. 17: 351–358.
36. Gijzen, F.J.H., E. Allanic, V.D. Vosse, J.D. Janssen. 1999. "The influence of the non-Newtonian properties of blood on the flow in large arteries: unsteady flow in a 90° curved tube." *J. Biomech*. 32: 705–713.

37. Johnston. B.M., P.R. Johnston, S. Corney, D. Kilpatrick. 2005. "Non-Newtonian blood flow in human right coronary arteries: Transient simulations." *J Biomech.* 39: 1116–1128.
38. Cho, Y.I., K.R. Kensey. 1991. "Effects of the Non-Newtonian viscosity of blood on flows in a diseased arterial vessel. Part 1: Steady flows." *Biorheology.* 28: 241–262.
39. Perktold. K., R.O. Peter, M. Resch. 1989. "Pulsatile non-Newtonian blood flow simulation through a bifurcation with an aneurysm." *Biorheology.* 26: 1011–1030.
40. Tang, D., C. Yang, S. Kobayashi, D.N. Ku. 2001. "Steady flow and wall compression in stenotic arteries: a three-dimensional thick-wall model with fluid–wall interactions." *Journal of Biomechanical Engineering.* 123: 548–557.
41. Tu, C., M. Deville. 1996. "Pulsatile flow of non-Newtonian fluids through arterial stenoses." *Journal of Biomechanics.* 29: 899–908.
42. Chan, W.Y., Y. Ding, J.Y. Tu. 2007. "Modeling of non-Newtonian blood flow through a stenosed artery incorporating fluid–structure interaction." *ANZIAM Journal.* 47 (EMAC2005): C507–C523.
43. Sankar, D.S., U. Lee. 2009. "Mathematical modeling of pulsatile flow of non-Newtonian fluid in stenosed arteries." *Communications in Nonlinear Science and Numerical Simulation.* 14 (7): 2971–2981
44. Shaw, S., R.S. R. Gorla, P.V.S.N. Murthy, C.O. Ng. 2009. "Pulsatile Casson fluid flow through a stenosed bifurcated artery." *International Journal of Fluid Mechanics Research.* 36 (1): 43–63.
45. Razavi, A., E. Shirani, M. Sadeghi. 2011. "Numerical simulation of blood pulsatile ow in a stenosed carotid artery using different rheological models." *Journal of Biomechanics.* 44 (11): 2021–2030.
46. Holdsworth. D.W., C.J.D. Norley, R. Frayne, D.A. Steinman, B.K. Rutt. 1999. "Characterization of common carotid artery blood-flow waveforms in normal subjects." *Physiological Measurements.* 20: 219–240.
47. Bloch, K. E., B. P. Krieger, and M. A. Sackner. 1991. "Noninvasive measurement of central venous pressure by neck inductive plethysmography." *Chest.* 100: 371–375.

48. Lou Z. and W.J. Yang, 1990. "A computer simulation of the blood flow at the aortic bifurcation with flexible walls." *Journal of Biomechanical Engineering*. 115: 306–315.
49. Nguyen, T.T., Y. Biadillah, R. Mongrain, J. Brunette, J.C. Tardif, O.F. Bertrand. 2004. "A method for matching the refractive index and kinematic viscosity of a blood analog for flow visualization in hydraulic cardiovascular models." *Journal of Biomechanical Engineering*. 126: 529–535.
50. Brookshier, K.A., J.M. Tarbell. 1993. "Evaluation of a transparent blood analog fluid: Aqueous Xanthan gum/glycerin." *Biorheology*. 30: 107-116.
51. Valencia, A., A. Zarate, M. Galvez. and L. Badilla. 2006. "Non-Newtonian flow dynamics in a right internal carotid artery with a saccular stenosis." *International Journal of Numerical Methods Fluids*. 50: 751–764.
52. Varghese, S.S., S.H. Frankel and P. Fischer. 2007. "Direct numerical simulation of stenotic flows, part I: steady flow." *Journal of Fluid Mechanics*. 582: 253–280.
53. Varghese, S.S., S.H. Frankel and P. Fischer. 2007. "Direct numerical simulation of stenotic flows, part I: steady flow." *Journal of Fluid Mechanics*. 582: 281–318.
54. Gijsen, F.J.H., F.N. van de Vosse and J.D. Janssen. 1999. "The influence of non-Newtonian properties of blood on the flow in large arteries." *Journal of Biomechanics* 32: 601-608.
55. Tada, S. and J.M. Tarbel. 2006. "Oxygen mass transport in a compliant carotid bifurcation model." *Annals of Biomedical Engineering*. 34(9): 1389-99.
56. Somkid A., B. Wiwatanapataphee, Y.H. Wu, Y. Lenbury. 2005. "Effect of non-Newtonian behaviour of blood on pulsatile flows in stenotic arteries." *International Journal of Biological and Life Sciences*. 1:1: 42:46.

APPENDIX

Appendix A: UDF for Inlet Boundary

```
#include"udf.h"

#include"math.h"

#define index 0.9

#definealph 15.81

#define n 0.0736

#define N .005

#define mu 0.00384

DEFINE_PROFILE(transient_velocity, thread, position)

{

    inti ;

    float t, velocity,a[100],b[100];

    face_t f;

    a[0]=0.000000;

    a[1]=0.836867;

    a[2]=0.097972;

    a[3]=-0.134835;

    a[4]=-0.301058;

    a[5]=-0.243957;

    a[6]=-0.178316;

    a[7]=-0.199582;
```

a[8]=-0.188538;
a[9]=-0.133882;
a[10]=-0.053157;
a[11]=0.051542;
a[12]=0.061436;
a[13]=0.096633;
a[14]=0.009737;
a[15]=-0.024491;
a[16]=0.014157;
a[17]=0.037180;
a[18]=-0.020342;
a[19]=-0.037159;
a[20]=-0.005900;
a[21]=-0.010321;
a[22]=-0.024950;
a[23]=-0.005907;
a[24]=0.008071;
a[99]=-0.00147;

b[0]=10.387075;
b[1]=1.850111;
b[2]=1.342319;

b[3]=0.898353;
b[4]=0.571498;
b[5]=0.486233;
b[6]=0.232850;
b[7]=0.052111;
b[8]=-0.035078;
b[9]=-0.091453;
b[10]=-0.076763;
b[11]=-0.054678;
b[12]=-0.011458;
b[13]=-0.002826;
b[14]=0.005890;
b[15]=0.069500;
b[16]=0.084245;
b[17]=0.052087;
b[18]=0.012200;
b[19]=0.039800;
b[20]=0.024575;
b[21]=-0.021485;
b[22]=-0.031720;
b[23]=0.000865;
b[24]=-0.011767;

```

b[99]=0.00174;

t = RP_Get_Real("flow-time");

velocity = b[0]+b[100]*cos(2*3.14159*(100)*t);

for (i=1;i<=24;i++)
{
    velocity = velocity +
    2*(a[i]*sin(2*3.14159*(i)*t)+b[i]*cos(2*3.14159*(i)*t));
}

begin_f_loop(f, thread)
{
    F_PROFILE(f, thread, position) = (velocity*.01)/(3.14159*.25);
}

end_f_loop(f, thread)
}

```

Appendix B: UDF for material properties of Visco-elastic fluid

```

DEFINE_PROPERTY(material_property,cell,thread)
{
    float trace;

    float visc,k;

    float u[3], v[3], w[3],l;

    int j;

```

```

for(j=0;j<3;j++)
{
    u[j]=C_U_G(cell,thread)[j];
    v[j]=C_V_G(cell,thread)[j];
    w[j]=C_W_G(cell,thread)[j];
}
trace=0.5*(2*pow(u[0],2)+pow(v[0]+u[1],2)+2*pow(v[1],2)+pow(v[2]+w[1],2)
+2*pow(w[2],2)+pow(w[0]+u[2],2));
k=(pow(0.5*(pow(trace,2)),.5));
l = 1+alph*k;
visc = N + (n-N)*(1+log(l))/l;
return visc;}

```